

Article

# Chemical Analysis of Lipid Boundaries after Consecutive Growth and Division of Supported Giant Vesicles

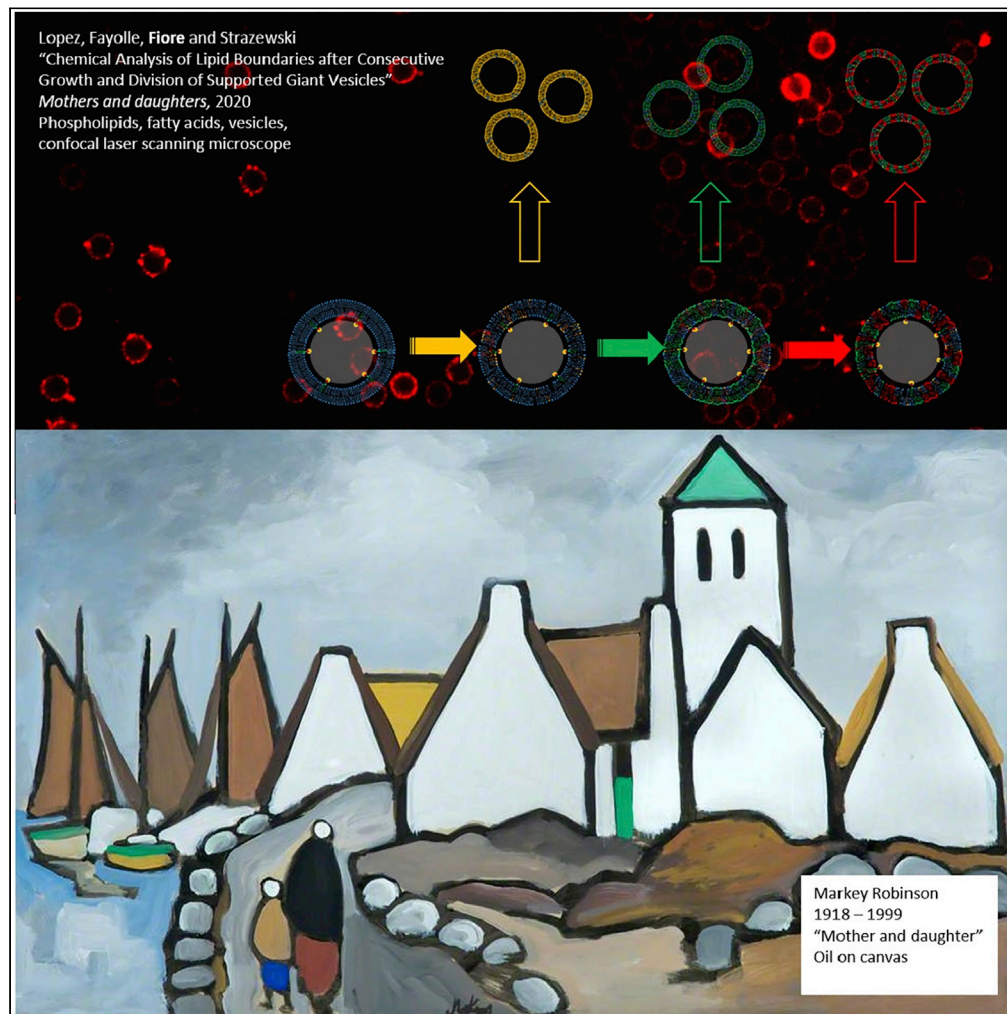


Figure360> For a Figure360 author presentation of this figure, see <https://doi.org/10.1016/j.isci.2020.101677>.

Augustin Lopez,  
Dimitri Fayolle,  
Michele Fiore,  
Peter Strazewski

michele.fiore@univ-lyon1.fr

**HIGHLIGHTS**  
 Protocellular model  
 membranes

Growth & Division

Self-evolving molecular  
 systems



## Article

## Chemical Analysis of Lipid Boundaries after Consecutive Growth and Division of Supported Giant Vesicles

Augustin Lopez,<sup>1</sup> Dimitri Fayolle,<sup>1</sup> Michele Fiore,<sup>1,2,\*</sup> and Peter Strazewski<sup>1</sup>

## SUMMARY

The reproduction of the shape of giant vesicles usually results in the increase of their "population" size. This may be achieved on giant vesicles by appropriately supplying "mother" vesicles with membranogenic amphiphiles. The next "generation" of "daughter" vesicles obtained from this "feeding" is inherently difficult to distinguish from the original mothers. Here we report on a method for the consecutive feeding with different fatty acids that each provoke membrane growth and detachment of daughter vesicles from glass microsphere-supported phospholipidic mother vesicles. We discovered that a saturated fatty acid was carried over to the next generation of mothers better than two unsaturated congeners. This has an important bearing on the growth and replication of primitive compartments at the early stages of life. Microsphere-supported vesicles are also a precise analytical tool.

## INTRODUCTION

Studying the self-reproduction (Stano and Luisi, 2010; Szostak, 2017) of lipidic giant vesicles (GVs) (Walde et al., 2010) is crucial for understanding the replication of prebiotic compartments in autopoietic systems (Varela et al., 1974). This replication of shapes and objects can result from a growth and division (G&D) process: feeding the lipid boundary of a mother vesicle with amphiphilic compounds induces its growth in size and eventually its division into daughter vesicles (Figure 1) (Stano and Luisi, 2010; Szostak, 2017). In pioneering studies, G&D of oleic acid vesicles was carried out by feeding them with oleic anhydride that rapidly inserted into the pre-existing membranes and hydrolyzed to oleic acid and oleate at basic pH (Figure 1A). The size of these vesicles and the G&D steps have been analyzed by microscopy (Walde et al., 1994; Wick et al., 1995). In more recent investigations, a wider variety of synthetic protocells have been used to describe the phenomenon (Lopez and Fiore, 2019; Matsuo et al., 2020, 2019; Ruiz-Mirazo et al., 2014; Schwille, 2019). For instance, the observation of mother vesicles encapsulating a ferritin cargo (Berclaz et al., 2001a, 2001b) or fluorescent probes (Hanczyc et al., 2003; Zhu and Szostak, 2009) assessed their division through the distribution of their content in daughter vesicles (Figure 1B). Furthermore, GV's composed of membranes that contained two different fluorescent probes allowed to monitor their growth in size by measuring the Förster Resonance Energy Transfer (FRET) effect (Figure 1C) that took place when the membranes budded (Chen, 2004; Hanczyc et al., 2003). Other techniques such as free-flow electrophoresis enabled the chemical characterization of the vesicles obtained after a single reproduction and sorting according to their charges (Pereira de Souza et al., 2015). However, one of the major issues in studying the G&D of GV's is the impossibility to distinguish and to separate mother from daughter vesicles after the replication step. Indeed, despite the fact that the different steps of the G&D process are known, for instance, budding, evagination, tubing, pearling, dumbbell formation, and division (Figure S1), most of the lipid exchange, which actually occurs between the vesicles and the medium during the phenomenon, remains uncertain. A clear separation of mother and daughter vesicles would allow one to independently characterize their lipid compositions in order to describe more precisely and reliably the lipid movements. The use of surface-mediated vesicle replication allows for the distinction of mother from daughter vesicles after a G&D process. However, only a few examples were reported in the literature. Vesicles can be anchored to a surface by either a specific integral membrane-bound linkage or through adsorption (Rebaud et al., 2014). Vesicles may be tethered to an avidin-coated surface via biotinylated phospholipids (Pignataro et al., 2000). Surface-attached vesicles would grow through the uptake of additional membrane components such as fatty acids in the form of free molecules or micelles, or through the fusion of added phospholipid vesicles. Vesicles adsorbed to a glass surface coated with hydrocarbons have also been shown to fuse with additional vesicles that were provided from a fluid flowing above. In that

<sup>1</sup>Université de Lyon, Université Claude Bernard Lyon 1, Institut de Chimie et Biochimie Moléculaires et Supramoléculaires, Bâtiment Edgar Lederer, 1 Rue Victor Grignard, 69622 Villeurbanne Cedex, France

<sup>2</sup>Lead Contact

\*Correspondence: [michele.fiore@univ-lyon1.fr](mailto:michele.fiore@univ-lyon1.fr)  
<https://doi.org/10.1016/j.isci.2020.101677>



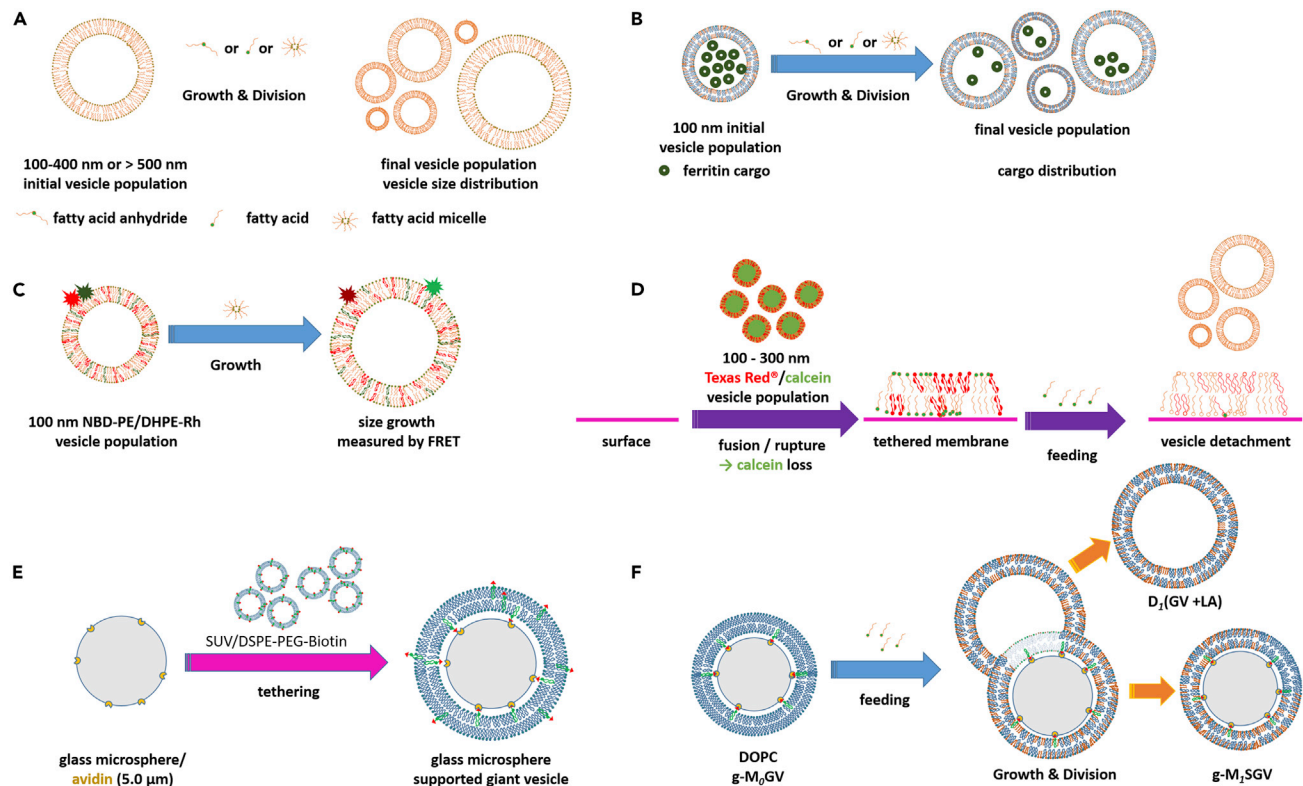


**Figure 1. Reported Experiments on Vesicles Formed from Membrane Growth and/or Self-Reproduction Processes**

(A) Growth and division of fatty acid (orange amphiphiles) vesicles (Walde et al., 1994; Wick et al., 1995).  
 (B) Cargo distribution after growth and division (Berclaz et al., 2001a, 2001b; Hanczyc et al., 2003; Zhu and Szostak, 2009).  
 (C) Vesicle growth observed by FRET (Chen, 2004; Hanczyc et al., 2003). Examples (A)–(C) do not allow for any distinction between mother and daughter vesicles.  
 (D) Tethered membranes and daughter vesicles formed by feeding glass or silica surface with fluorescent vesicles (Johnson et al., 2002; Morigaki and Walde, 2002).  
 (E) Preparation of glass microsphere-supported giant phospholipid (blue amphiphiles) vesicles (Gopalakrishnan et al., 2009).  
 (F) Growth and detachment of membranes using supported giant vesicles allow distinction and separation of mothers from daughters (Albertsen et al., 2014; Fiore et al., 2018).

case, a microfluidic device delivered phospholipidic vesicles of 30–100 nm diameter that were adsorbed to and fused with the tethered lipidic quartz surface. Two-color fluorescence signatures were used to monitor the process (Johnson et al., 2002). This process was also observed by Morigaki and Walde when fatty acid micelles were delivered instead of phospholipid vesicles (Morigaki and Walde, 2002).

We have found that glass microsphere-supported giant vesicles (g-MSGVs), being GVs filled with a functionalized glass bead of a defined size (5.0 μm) bearing a tethered membrane around this glass core (schematized in Figure 2A), can generally serve to monitor the lipids during several generations of the G&D process. We have observed that G&D arises from the budding and eventually detachment of lipid membranes that aggregate to a significant part into daughter vesicles, alike the corresponding process occurring from non-supported vesicles, commonly studied as models for protocells (Albertsen et al., 2014; Chen, 2004; Hanczyc et al., 2003; Hardy et al., 2015; Lopez and Fiore, 2019; Terasawa et al., 2012; Tomita et al., 2011; Walde et al., 1994; Wick et al., 1995; Zhu and Szostak, 2009). Such supported membrane boundaries can be submitted to several distinct feeding processes, just as any phospholipidic vesicles can, yet with the advantage of being able to separate unambiguously the daughter vesicles formed after a G&D process from the left-over surface-supported mother vesicles by centrifugation (Fiore et al., 2018). The first preparation of this construct was reported by Gopalakrishnan et al. (2009) by means of a mixture of phospholipids anchored to a substrate thanks, again, to an avidin/biotin interaction (Pignataro et al., 2000). G&D was performed by Monnard and co-workers who used decanoic acid/decanoate membranes supported on the same monodisperse glass bead microspheres of 5.0 μm

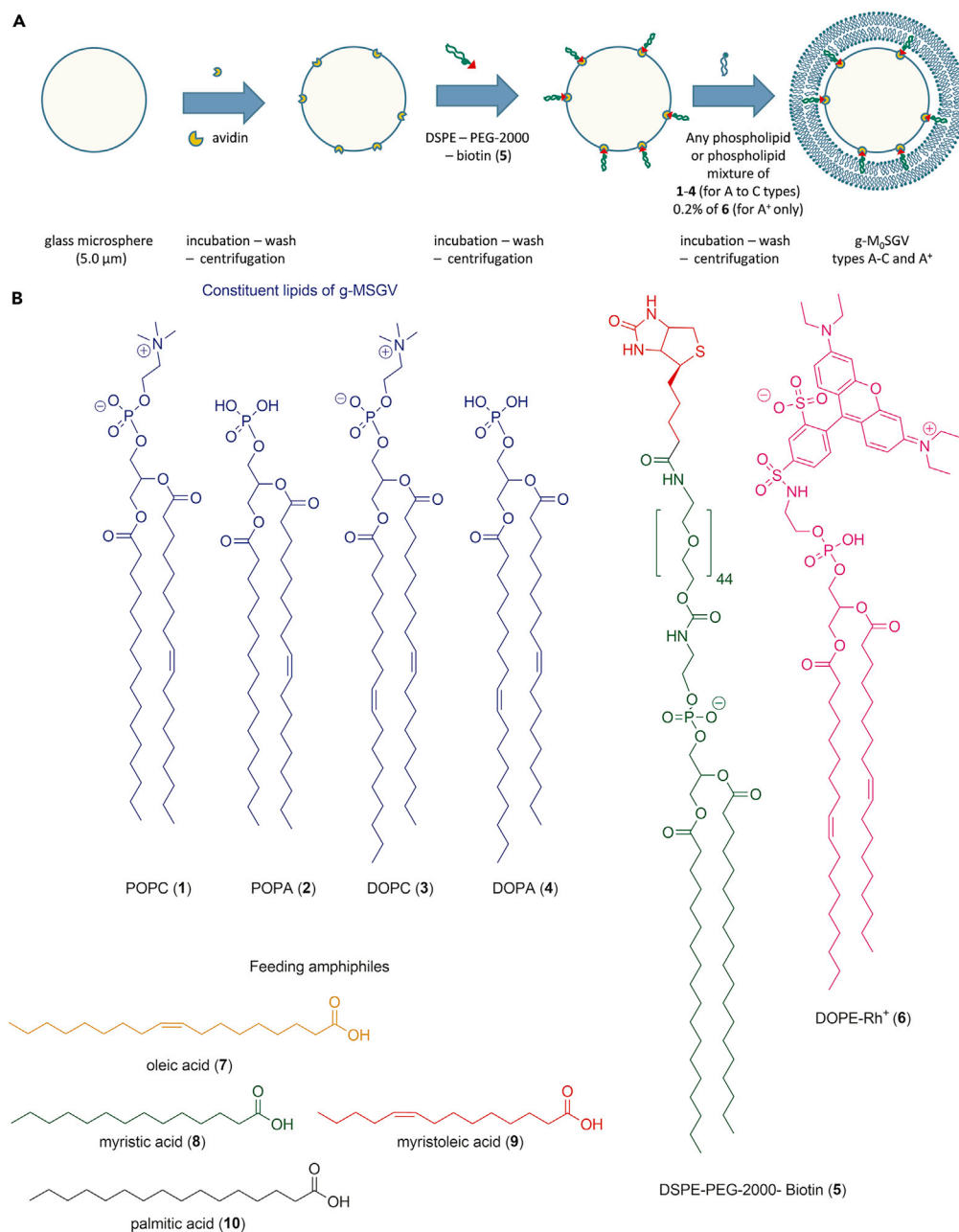


**Figure 2. Process for Coating g-M<sub>0</sub>SGVs with Different Phospholipids Using Our Method and Structure of Used Amphiphiles**

(A) Glass microspheres were first tethered with avidin/biotinylated phospholipid, then coated with phospholipids (Fiore et al., 2018).

(B) Structure of the phospholipids 1–6 (without counterions for clarity) used for preparation of g-M<sub>0</sub>SGVs and fatty acids 7–10 used for feeding supported vesicles. Color code serves to distinguish phospholipids from fatty acids in the following figures.

diameter that we are presenting here (Albertsen et al., 2014). We reasoned that we could combine these separate studies to answer the question: how can the compositional dynamics during consecutive G&D processes of phospholipid boundaries be followed experimentally? Here we provide an optimization of our previously described method (Fiore et al., 2018), that is, a general tool for chemically monitoring the lipid exchange that occurs during several consecutive G&D processes.

One key feature of the g-MSGVs is their higher density, owing to the glass bead inside, allowing for their separation by centrifugation from all lipid material floating in the host solution. Fatty acids, when supplied to g-MSGVs, partitioned into their phospholipidic boundary. This made their boundary grow in size until a fragment eventually detached to generate, among others, giant daughter vesicles (DGVs), whereas regularly sized supported mother vesicles with altered membrane composition were left behind. The heavier mother vesicles could be thus isolated from all lipids that detached from the mothers. The initial preparation of the g-MSGVs covered with phospholipids (DOPC) was recently reported (Fiore et al., 2018). Phospholipids with a low critical vesicle concentration (cvc) (Zhou et al., 1999) (phospholipids 1–4, Figure 2B) were anchored to glass microspheres using a chemical architecture made of avidin and biotin-DSPE (5, Figure 2B). The g-MSGVs were classified based on their phospholipidic composition; the list of the supported vesicles used in this study is reported in Tables 1 and S1. POPC, DOPC, POPA, and DOPA were blended in different ratios. Pure POPC membranes were named A type, a blended binary mixture of POPC-POPA (4:1 molar ratio) B type, and quaternary mixtures from POPC-POPA-DOPC-DOPA (4:1:4:1 molar ratio) C type (Tables 1 and S1). Type A<sup>+</sup> g-MSGVs (POPC, Table S1) containing additional 0.2 mol % DOPE-Rh (6, Figure 2B) served for their observation under the confocal microscope to evidence G&D (cf. Figure 3B). Supported vesicles containing phosphocholine extracts from soybean and egg yolk (g-MSGVs D and E, Table S1) were prepared as well. However, in order to limit the complexity of the system, these two populations of g-MSGVs bearing a tethered “natural” membrane were not used for consecutive feeding experiments as described below. The visual aspect of the supported vesicle samples was the same whatever were their composition (Table S1, Figure S2). Noteworthy, after the final washing step (phase 3, Figure 2B) no floating vesicles were observed in the hosting solution (HS) (Figure S2). Four fatty acids (7–10, Figure 2B) were selected as feeding molecules. Our choice was based on the results reported by Luisi and Szostak (Stano and Luisi, 2010; Szostak, 2017). In addition, two synthetic lipophilic and fluorescent probes  $\omega$ -(dansyl)laurinyl derivative 11 and  $\delta$ -(isopropanylidene)tryptophanyl derivative 12 (Schemes S1 and S2 and Figures S16–S21) were used. The growth and partial detachment of lipid boundaries from g-MSGVs of all membrane types A–E were followed by microscopy. Owing to precipitation issues with the amphiphiles 10–12 (Table 1, Entries 6–9), only oleic, myristic, and myristoleic acids (7–9 Figure 2B) were kept for consecutive feeding in G&D experiments. We optimized the feeding of g-MSGVs by using ethanolic solutions of 7–9 at 10, 25, and 50 mM concentrations. Myristic acid (8) also precipitated but only when a 50 mM feeding solution was used. A 10 mM initial feeding concentration was chosen as it produced in preliminary test feedings an approximative 1:1 partitioning of the phospholipids between the first-generation g-MSGVs and the lipids in the hosting solution (Figure S3). This 1:1 ratio was not reproduced later in more systematic tests (cf. Figures 4 and 5 and Table 1). During each feeding period ethanol evaporated only gradually, thus, it kept the fatty acids as free compounds, which avoided for some time the formation of micelles or other aggregates (Walde et al., 2010). Control experiments when g-MSGVs were fed with pure ethanol showed no detachment of phospholipids in solution by microscopy (Fiore et al., 2018). The feeding ratio was tuned to 33  $\mu$ L/h and the total feeding time 3 h. The selected parameters minimized the early *de novo* formation of aggregates, thus permitted to reach a total concentration of 1 mM of 7–9 in the HS.

To stay unambiguous and clear at the same time, we renamed the g-MSGVs as g-M<sub>n</sub>SGVs, where g stands for glass, M stands for “microsphere” or “mother,” and the subscript *n* is an increasing positive integer for M<sub>1</sub>, M<sub>2</sub>, M<sub>3</sub> to distinguish each mother population generated from each feeding process (Figure 3A). The initial population of g-MSGVs was named g-M<sub>0</sub>SGVs. With DGVs, where D stands for “daughter,” we designated the floating vesicles generated from a first, second, or third G&D process, so, accordingly, an increasing subscript integer for D<sub>1</sub>, D<sub>2</sub>, D<sub>3</sub> appointed each generation of the population of daughters. With time passing after each feeding step, we observed to a varying degree the appearance of floating aggregates of lipids that accompanied the daughter vesicles. Therefore, we used the abbreviation D(GV + LA) to designate all floating lipid material in the HS, where LA stands for other lipid aggregates. After each G&D process, the supported mother vesicles g-M<sub>1-3</sub>SGVs were isolated by sequential cycles of centrifugation and washings from all floating lipids D<sub>1-3</sub>(GV + LA)s (Figure 3A). In this study, we took advantage of these model giant vesicles to independently characterize the lipid composition of the g-M<sub>n</sub>SGVs and the D<sub>n</sub>(GV+LA)s after every successive feeding experiment (results in Figure 4 and Table 1). The model diagram below the images in Figure 3B is meant as a guide that puts images taken at about the same time (Figure 3B, images a-d) into an assumed process-dependent context. It does not imply an actual time lapse following of the same g-MSGV in a, b, c, and d. The phospholipids and fatty acids were extracted with chloroform (Bligh and Dyer, 1959). RP-HPLC (Heron et al., 2007) served to quantify the composition of fatty acids after one, two, or three consecutive feeding processes (Table 1). The Stewart assay (Stewart, 1980), even if

Entry	g-M <sub>0</sub> SGVs <sup>a</sup>	Microscopic Observations <sup>b</sup>	Vesicles Product	PL Concentration <sup>c,d</sup> (mM)	PL <sub>found</sub> /PL <sub>initial</sub>	1 <sup>st</sup> Feeding	2 <sup>nd</sup> Feeding	3 <sup>rd</sup> Feeding	Final Composition
						7 <sub>found</sub> /7 <sub>fed</sub> <sup>d,e</sup>	8 <sub>found</sub> /8 <sub>fed</sub> <sup>d,e</sup>	9 <sub>found</sub> /9 <sub>fed</sub> <sup>d,e</sup>	
1	A (1)	Budding, Growth, Pearling, and Division	D <sub>1</sub> (GV + LA)s	0.18 ± 0.01	0.33 ± 0.01	0.90 ± 0.01	–	–	1 + 7
			D <sub>2</sub> (GV + LA)s	0.17 ± 0.01	0.31 ± 0.01	0.06 ± 0.02	0.68 ± 0.01	–	1 + 7+8
			g-M <sub>2</sub> SGVs	0.20 ± 0.01	0.36 ± 0.01	0.04 ± 0.01	0.32 ± 0.01	–	1 + 7+8
2	A (1)	Budding, Growth, Pearling, and Division	D <sub>1</sub> (GV + LA)s	0.14 ± 0.01	0.25 ± 0.01	0.91 ± 0.03	–	–	1 + 7
			D <sub>2</sub> (GV + LA)s	0.15 ± 0.01	0.27 ± 0.02	0.03 ± 0.01	0.54 ± 0.03	–	1 + 7 + 8
			D <sub>3</sub> (GV + LA)s	0.13 ± 0.01	0.24 ± 0.01	0.03 ± 0.01	0.33 ± 0.01	0.76 ± 0.05	1+7-9
			g-M <sub>3</sub> SGVs	0.13 ± 0.01	0.24 ± 0.01	0.03 ± 0.01	0.13 ± 0.02	0.24 ± 0.05	1+7-9
3	B (1 + 2)	Budding, Growth, Pearling, and Division	D <sub>1</sub> (GV + LA)s	0.20 ± 0.01	0.37 ± 0.01	0.89 ± 0.03	–	–	1 + 2+7
			D <sub>2</sub> (GV + LA)s	0.16 ± 0.02	0.28 ± 0.03	0.08 ± 0.02	0.65 ± 0.03	–	1 + 2+7 + 8
			g-M <sub>2</sub> SGVs	0.19 ± 0.01	0.35 ± 0.02	0.03 ± 0.01	0.35 ± 0.03	–	1 + 2+7 + 8
4	C (1–4) <sup>f</sup>	Budding, Growth, Pearling, and Division	D <sub>1</sub> (GV + LA)s	0.11 ± 0.01	0.20 ± 0.01	0.99 ± 0.03	–	–	1-4+7
			D <sub>2</sub> (GV + LA)s	0.34 ± 0.02	0.62 ± 0.03	0.008 ± 0.0001	0.57 ± 0.03	–	1-4+7 + 8
			g-M <sub>2</sub> SGVs	0.10 ± 0.01	0.18 ± 0.02	0.002 ± 0.001	0.43 ± 0.03	–	1-4+7+8
Inverted Feeding Order			Vesicles Product	PL Concentration <sup>c,d</sup>	PL <sub>found</sub> /PL <sub>initial</sub>	1 <sup>st</sup> Feeding	2 <sup>nd</sup> Feeding	Final Composition	
Entry	g-M <sub>0</sub> SGVs <sup>a</sup>	Microscopic Observations <sup>b</sup>				8 <sub>found</sub> /8 <sub>fed</sub> <sup>d,e</sup>	7 <sub>found</sub> /7 <sub>fed</sub> <sup>d,e</sup>		
5	A <sup>+</sup> (1)	Budding, Growth, Pearling, and Division	D <sub>1</sub> (GV + LA)s	0.20 ± 0.02	0.37 ± 0.04	0.43 ± 0.01	–	–	1 + 8
			D <sub>2</sub> (GV + LA)s	0.18 ± 0.02	0.33 ± 0.04	0.45 ± 0.02	0.95 ± 0.01	–	1 + 8+7
			g-M <sub>2</sub> SGVs	0.17 ± 0.02	0.30 ± 0.03	0.12 ± 0.01	0.05 ± 0.01	–	1 + 8+7
Other Feedings			Fed with	Vesicles Product					Final Composition
Entry	g-M <sub>0</sub> SGVs <sup>a</sup>								
6	A (1)		10	None/aggregates					–
7	A (1)		11	None/aggregates					–
8	A (1)		12	None/aggregates					–

**Table 1. Microscopic and Chemical Analysis of Lipid Boundaries Content after Two or Three Consecutive Feeding Experiments on D<sub>1</sub>(GV + LA)s, D<sub>2</sub>(GV + LA)s, D<sub>3</sub>(GV + LA)s, g-M<sub>2</sub>SGVs, and g-M<sub>3</sub>SGVs by Using g-M<sub>0</sub>SGVs Type A–C**

<sup>a</sup>1=POPC, 2=POPA; 3=DOPC, 4=DOPA, 7=oleic acid, 8=myristic acid, 9=myristoleic acid.

<sup>b</sup>Descriptions and images of the phenomena are available in the [Supplementary Information](#).

<sup>c</sup>Concentrations of phospholipids 1, 2, 3, and 4 measured by Stewart assay and normalized to 0.55 mM.

<sup>d</sup>Mean values and standard errors were determined from experiments performed in triplicates (n=3).

<sup>e</sup>Concentration of fatty acids 7, 8, and 9 measured by HPLC and normalized to 1 mM.

<sup>f</sup>Analysis of the lipid boundaries containing soybean and egg-yolk extracts (Table S1, entries 5 and 6, D and E types, respectively) was not performed. C type MSGVs can be considered as a simplified model of D and E type coatings.

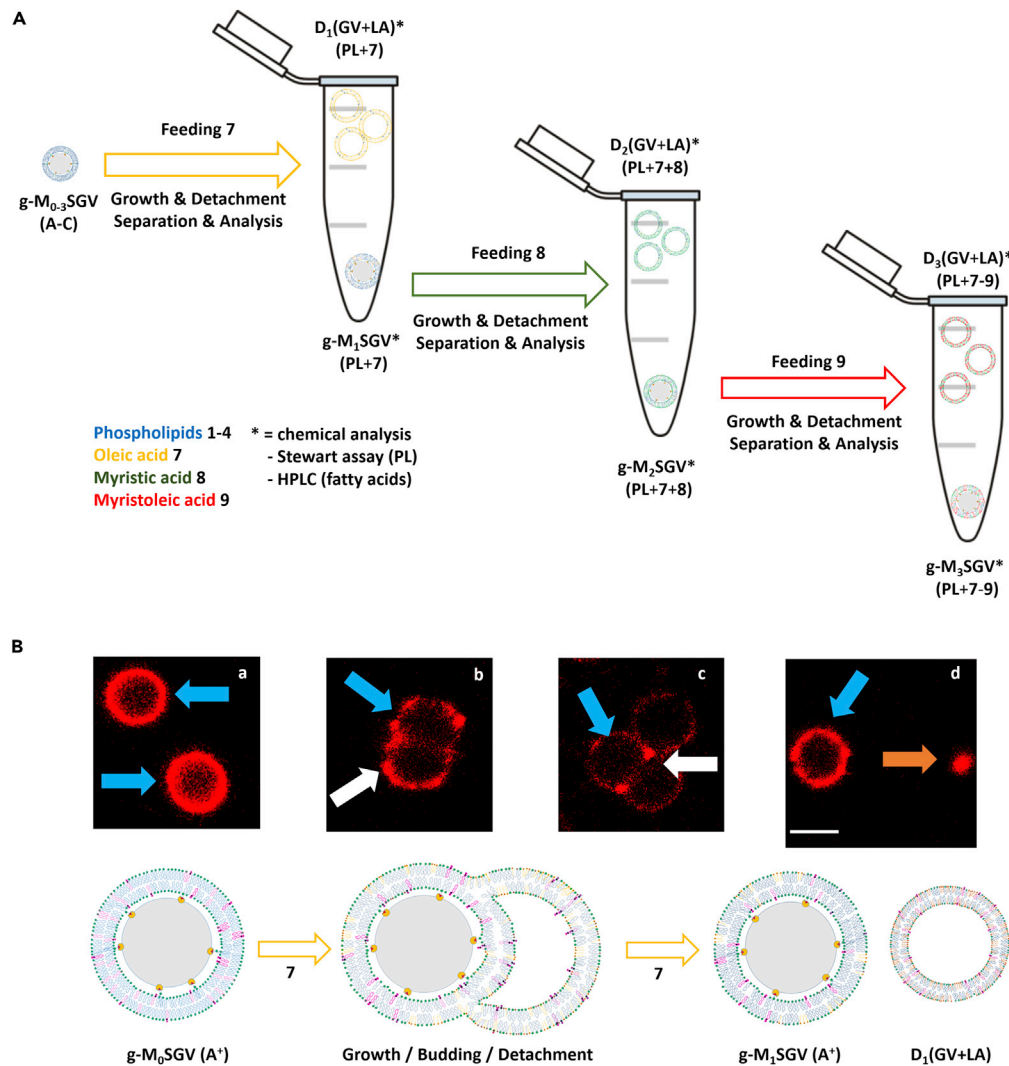


**Figure 3. Experimental Setup and Representative Microscopic Results**

(A) Workflow of monitoring of three consecutive feeding processes on phospholipid-coated glass beads, that is, glass microsphere-supported giant vesicles (g-M<sub>0</sub>SGVs, A-C type coatings) fed with fatty acids.

(B) Micrographs of periodic microscopic confocal observations during feeding of POPC g-M<sub>0</sub>SGVs bearing 0.2% red fluorescent DOPE-Rh (see MPB in [Transparent Methods](#)). The confocal microscope images do not correspond to a time-lapse monitoring of a single g-M<sub>1</sub>SGV. They show different objects that are thought to represent the most prominent stages of a G&D model process as shown schematically below: (a) A<sup>+</sup> type g-M<sub>0</sub>SGVs ([Table S1](#), entry 3) before feeding; (b) budding (60 min); (c) membrane growth (60 min); (d) detachment with apparition of a daughter vesicle (D<sub>1</sub>GV, 60 min). Blue arrows indicate g-M<sub>1</sub>SGVs, white arrows indicate the G&D phenomena, and orange arrow indicates recently formed daughter vesicle. Pictures were accompanied by a simplified draw, below the confocal images, that resume the most important phases observed during feeding experiments: The scale bar is 5 μm for all images.

less precise than an HPLC analysis, was used to determine, independently of the fatty acid quantification, the initial ([Table S2](#)) and final ([Table 1](#)) concentrations of phospholipids (PLs) in g-M<sub>0</sub>SGVs, g-M<sub>2-3</sub>SGVs, and D<sub>1-3</sub>(GV + LA)s, respectively. All experiments were performed in triplicate, and these data were used to calculate the mean concentrations and the associated standard deviations ([Table 1](#)).

## RESULTS

Prior to any chemical analysis, we monitored that G&D was indeed occurring. The main types of phenomena described during the growth of a lipid boundary upon feeding were budding, growth (in size), pearling, and division/detachment ([Figure S1](#)) ([Stano and Luisi, 2010](#); [Szostak, 2017](#)). They all happened upon addition of oleic,

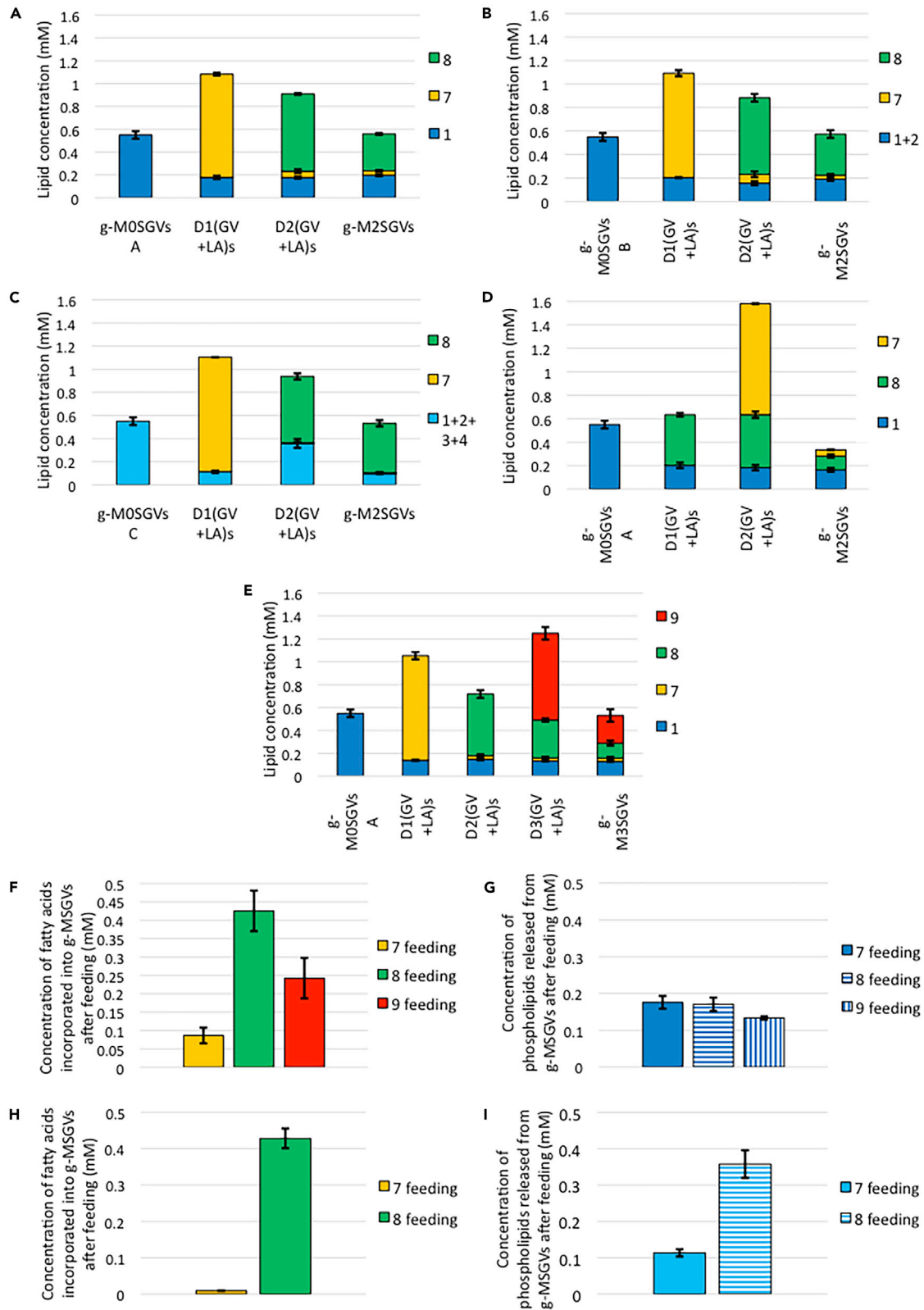


**Figure 4. Graphical Representation of the Data Obtained from the Analysis of g-M<sub>n</sub>SGVs and D<sub>n</sub>(GVs+LA)s after Consecutive Growth and Division of Supported Giant Vesicles**

(A–E) Concentrations (mM) of phospholipids and fatty acids in g-M<sub>0</sub>SGVs, D<sub>1-3</sub>(GVs + LA)s and g-M<sub>2-3</sub>SGVs after two or three feeding periods. Composition of g-M<sub>0</sub>SGVs: (A), (D), (E) POPC (1, A type coating); (B) POPC/POPA 4:1 (1 + 2, B type coating); (C) POPC/POPA/DOPC/DOPA 4:1:4:1 (1 + 2+3 + 4, C type coating). Feeding order: (A–C) first oleic acid (7) then myristic acid (8); (D) first 8 then 7; (E) first 7 then 8 then myristoleic acid (9).

(F–I) Concentrations (mM) of fatty acids incorporated into g-MSGVs (F and H); phospholipids released from g-MSGVs into HS (G and I), after respective feeding periods. Amounts and standard deviations obtained from Table 1: A and B type g-MSGVs grouped (sample size = 12) (F and G); C type g-MSGVs only (sample size = 3) (H and I). Concentration of incorporated fatty acids (F and H) corresponds to (i) amount found in g-M<sub>n</sub>SGVs if corresponding fatty acid was last supplied during feeding *n*, (ii) sum of amounts found in D<sub>*n*+1</sub>(GV + LA)s and g-M<sub>*n*+1</sub>SGVs when corresponding fatty acid was second to last supplied during feeding *n*, (iii) sum of amounts found in D<sub>*n*+1</sub>(GV + LA)s, D<sub>*n*+2</sub>(GV + LA)s and g-M<sub>*n*+2</sub>SGVs when corresponding fatty acid was third to last supplied during feeding *n*. Concentration of released phospholipids (G and I) corresponds to amount found in D<sub>*n*</sub>(GV+LA)s after supply with corresponding fatty acid during feeding *n*.

myristic, and myristoleic acids (7–9 Figures 2, 3B, and S8–S13). Of note, there were no remarkable differences between the different coating types of g-MSGVs (A–E, Table S1) during our observations by confocal (Figure 3B) and epifluorescence microscopy (Figures S8–S13). However, it appeared that oleic acid (7) induced more easily the G&D from g-MSGVs. The critical micelle concentration (CMC) of pure 7 is 1 mM, which is lower than the CMC of shorter fatty acids—the CMC of 8 is 15 mM—and in the range of the final concentrations at the end of the feeding (0–1 mM) (Budin et al., 2012). The critical aggregation concentrations (CACs) of pure 7 and 8 are 0.1 and 2 mM, respectively. In our opinion, owing to the relatively high expected critical vesicle concentration (CVC) of the fatty acids, and their relatively narrow pH and salt tolerance, only fatty acid micelles and aggregates were likely to form during the feeding process before they partitioned between the HS and the g-MSGV's membrane (Cape et al., 2011). Our choice for the feeding concentration and amount of added fatty acid generated final concentrations of at most 1 mM. This meant that the fraction of 7–9 that was not bound to the phospholipid membranes (the leftover fatty acids) could only be present in concentrations much below their respective CMC. However, the effective CAC, CMC, and CVC of fatty acid mixtures may become even lower in the presence of phospholipids. Therefore, some aggregates, micelles, and even vesicles could be present after the feeding period. Feeding supported giant vesicles with higher concentrations of fatty acid solutions (25 and 50 mM, Figure S3) expectedly produced more rapidly the same previously described phenomena (Figures S10–S13), although evagination was barely seen here (Figure S1), in contrast to what we described in our previous communication (Fiore et al., 2018).

We performed a set of experiments directly above the (inverted) lens of a confocal laser scanning microscope. The prepared POPC g-M<sub>0</sub>SGVs type A<sup>+</sup> membranes (Table S1) were initially expectedly spherical (Figure 3B, image a). The formation of buds was observed after feeding g-M<sub>0</sub>SGVs with oleic acid (25 mM ethanolic solution 7) (Figure 3B, image b). Such buds could increase in size during the growth step (Figure 3B, image c). Budding and membrane growth were observed at the same moment. We noticed that, in some cases, the fast local growth also induced the formation of lipid tubes (pearling) from g-M<sub>1</sub>SGVs, which were similar to those observed in the pearling phenomenon prior to the division of oleic acid vesicles (Figures S1 and S13) (Szostak, 2017; Zhu et al., 2012; Zhu and Szostak, 2009). Finally, we observed the formation of new vesicles (D<sub>1</sub>GVs, Figure 3B, image d) due to feeding with fatty acids. It was possible to ascertain that these new D<sub>1</sub>GVs were freshly formed from the g-M<sub>0</sub>SGVs, since they contained the fluorescent phospholipid probe 6 that was only added to the mother vesicles and shown not to leak even after prolonged time periods (Figure 3B, image d). Similar observations were also made when G&D processes were performed by feeding g-M<sub>0</sub>SGVs bearing phospholipid membranes of more complex B and C type compositions (Table S1, Figures S8–12).

After the confirmation that G&D was indeed occurring on our mother vesicles, we set out to monitor the lipid exchange between the g-M<sub>n</sub>SGVs and the medium during consecutive G&D. The phospholipid concentration of the g-M<sub>0</sub>SGVs was determined by the Stewart assay using B type g-M<sub>0</sub>SGVs (Table S1). This type of supported giant vesicles of binary compositional complexity was used as a reference for all the others, since the phospholipids (POPC and DOPC, POPA and DOPA) were fairly similar to one another (Figure 2B). An average concentration of 0.55 mM was measured for samples containing  $9 \times 10^5$  g-M<sub>0</sub>SGVs. This amount corresponded to  $3.7 \times 10^{11}$  phospholipid molecules coated on one single g-M<sub>0</sub>SGV and compared with a maximal coating of  $2 \times 10^8$  biotinylated tether molecules; hence, an at least 2,000-fold molar excess untethered over tethered phospholipids (Table S2). Surprisingly, the amount of coated phospholipid molecules was much higher than the one expected for unilamellar vesicles (Walde et al., 2010) and can be explained by the fact that the g-MSGVs formed could be at least partly multilamellar (Albertsen et

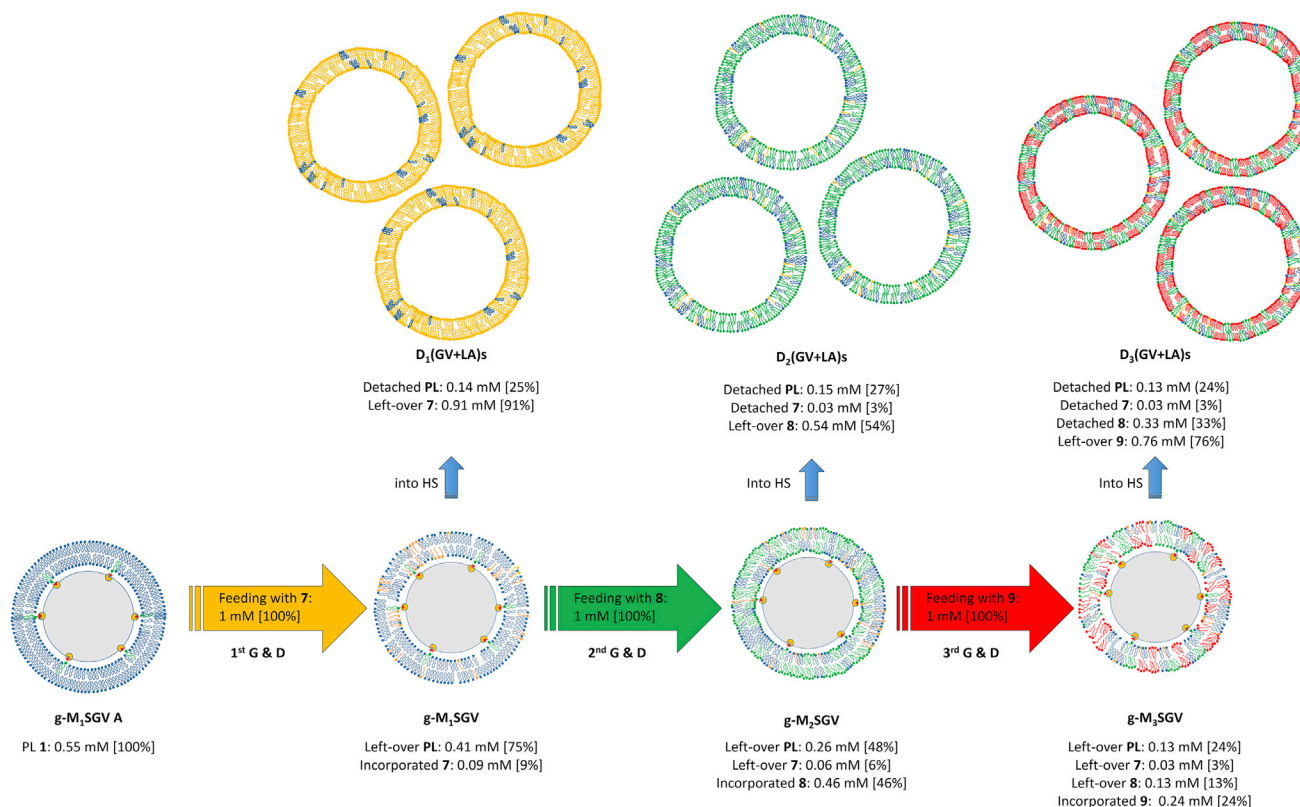


**Figure 5. Exemplary Pseudo-Molecular 2D Representation of Triple-Feeding Process Resulting in Measured and Deduced Phospholipid and Fatty Acid Concentrations and Partition Values**

Percentages in square brackets refer to concentration of phospholipids and fatty acids of g-M<sub>0-3</sub>SGVs and D<sub>1-3</sub>(GV + LA)s partitioned over A type mothers and daughters after each feeding step: (% = concentration of one amphiphile type/total concentration of this amphiphile type). Total concentration of PL (0.55 mM, 215 blue objects) corresponds to amount on g-M<sub>0</sub>SGVs. Total concentration of each fatty acid (1 mM, 390 yellow, green, or red objects) corresponds to supply during each respective feeding period. Object sizes not scaled, number of tethered molecules not proportional, multilamellarity not depicted.

al., 2014). Besides, the multilamellarity more readily explains the pearling phenomenon (Szostak, 2017; Zhu et al., 2012; Zhu and Szostak, 2009) that was observed during the G&D from g-MSGVs (Figure S12). The measured lipid concentrations were in general lower than expected. This was probably due to losses occurring during the extraction step. In order to compare the different conditions, the measured phospholipid concentrations were normalized to a total amount of 0.55 mM. This concentration corresponds to the initial amount present on the g-M<sub>0</sub>SGVs in the initial sample volume before feeding started, whereas the measured fatty acid concentrations were normalized to a total concentration of 1 mM corresponding to the amount supplied during one feeding period (Figure 4, Table 1).

The feeding of three different types of g-M<sub>0</sub>SGV membrane coatings (A, B, and C, Tables 1 and S1) was tested by performing two consecutive feedings, first with oleic acid (7) then myristic acid (8) (Figures 4A–4C, Table 1). We assumed that changing the nature of the membrane would impact the stability properties and the exchanges occurring between the g-MSGVs and the HS. Our results instead showed that the composition of the phospholipidic membranes did not seem to have any significant impact on the feeding with fatty acids (Figures 4A–4C and 5). Of note, when the first feeding was performed using C type g-MSGVs (Figure 4C), a higher amount of oleic acid (7) was found in the HS. Besides, the feeding with this fatty acid induced less detachment of phospholipids for C type g-MSGVs compared with A and B type g-MSGVs (Figures 4A and 4B). The second feeding with 8 released markedly more phospholipids from C type membranes, whereas the fatty acid concentrations were much the same for all types (Table 1, entries 1 and 3).

In the end, the three different populations of vesicles and floating lipid aggregates obtained, D<sub>1</sub>(GV + LA)s, D<sub>2</sub>(GV + LA)s, and g-M<sub>2</sub>SGVs, bore as membrane constituents a mixture of all the amphiphiles but in different

molar ratios (Figures 4A–4C and 5, and Table 1). However, the amount of 7 found in the most complex C type membranes (Table 1, entry 4) was the smallest when compared with both A and B type membranes (Table 1, entries 1 and 3). We assume that this observation is related to the fact that 7 hardly exchanged with the phospholipid membrane of the initial  $M_0$ SGVs of any membrane type A–C. In a situation where the kind of polar headgroups was constant in all types of phospholipid membranes, the difference in their acyl chains (1–4) apparently did not strongly influence the fatty acid uptake properties of the membranes.

As mentioned above, when A type g-MSGVs were first fed with oleic acid (7) then with myristic acid (8). 7 was much more present in the host solution containing  $D_2$ (GV + LA)s than 8 (Figure 4A). This result could be due to the fact that, during the second feeding, more room was available on the A type g- $M_1$ SGVs because their phospholipids progressively detached and were released to the host solution. To test this, the order of feeding was inverted. Curiously, we observed that the concentration of myristic acid (8) in the HS containing  $D_2$ (GV + LA)s was still lower than that of oleic acid (7) (Figure 4D). Thus, we could confirm that the saturated fatty acid 8 tended to stay more in the lipid membrane of the mother vesicles after a G&D when compared with the unsaturated fatty acid 7 (Figures 4A–4D). With these experiments it was also possible to observe that the compositional complexity of a membrane could increase owing to a continued feeding process because, rather than completely replacing one another, all different types of amphiphiles were present. The PC/PA headgroups (1–4), oleic and myristic acids (7, 8), were found in the membranes of the second-generation mother vesicles g- $M_2$ SGVs at the end of the experiments, that is, after being separated from their  $D_2$ (GV + LA)s (Table 1).

In order to observe whether the compositional complexity could reach yet another level and if unsaturated fatty acids were indeed more released in the host solution than saturated fatty acids, a third feeding was performed with myristoleic acid (9, Figure 4E). To this end, g- $M_2$ SGVs were generated from g- $M_0$ SGVs upon two consequent feedings with 7 and, respectively, 8 and those were supplied with 9. After this third feeding all amphiphiles (PL = 1, FA = 7–9) were detected as constituents of, both, mothers g- $M_3$ SGVs and daughters  $D_3$ (GV + LA)s in their respective membranes (Table 1, entry 2). Interestingly, we observed that, despite the same number of carbons present in the fatty acid chains, myristoleic acid (9) was more present in the host solution than myristic acid (8) after their respective feeding periods. Besides, after a G&D the incorporation of 9 was similar to that of 7 (oleic acid) and lower than that of 8 (Table 1). Thus, the unsaturated fatty acids 7 and 9 partitioned consistently less into the membranes of g- $M_0$ SGVs and g- $M_1$ SGVs after a G&D compared with the only tested saturated fatty acid 8.

## DISCUSSION

The use of giant vesicles filled with, and supported by, a monodisperse microspherical glass bead (g-MSGVs) allowed us to better understand the lipid exchange that occurred upon feeding the supported phospholipid membranes with fatty acids. For the quantification of lipid exchange we chose feeding conditions that in preliminary experiments (Figure S3) led to the detachment of at most one-half of the phospholipids from the zeroth-generation mother vesicles (g- $M_0$ SGVs) to generate membranes of daughter vesicles and some structurally less-defined aggregates. We did not separately quantify the lipids that were present in giant daughter vesicles (DGVs) from those that had formed other lipid aggregates (LA), but we could identify the microscopic difference between daughter vesicles and other aggregates present in the host solution only for objects larger than about 0.5  $\mu\text{m}$ . The low final feeding concentrations of the fatty acids favored their coexistence in the available phospholipid membranes and aggregates, which is consistent with the finding by others that fatty acids remain more firmly bound in phospholipid containing membranes than they would in pure fatty acid bilayer membranes (Jin et al., 2018). This paves the way for an assumed spontaneous rigidification and enrichment of prebiotic membranes bearing higher and higher amounts of phospholipids. Pure POPC membranes and those containing 20% POPA (coating types A and B, respectively) showed similar properties in incorporating fatty acids and detaching phospholipids (data grouped in Figures 4F and 4G). Those that contained 50% DOPC/DOPA 4:1 (C type coating) were particularly prone to be detached by myristic acid (8) but much less so by oleic acid (7) (Figures 4H and 4I). In Figure 5 the distribution of phospholipids and fatty acids in the triple-feeding experiment on A type membranes is depicted in a generation-dependent fashion, where the power of phospholipid detachment from mothers to daughters was related to the feeding material (for a more schematic graphical depiction of all distributions listed in and derived from Table 1 see Figures S14 and S15).

We focused our attention on the mother vesicles because of their obvious superior properties as evolvable micro-compartments in later generations. The growth in size, detachment, and closure of the grown membranes into

giant daughter vesicles reminds very strongly of what happens when “natural” unsupported giant vesicles grow in size then divide (G&D) into smaller daughter vesicles, thus, of vesicles that have grown in number after each feeding round and G&D process. Despite the fact that the type of membranes used for the supported vesicles did not really influence the fatty acid incorporation, we have shown that the type of fatty acid used as feeding material mattered indeed. Irrespective of the feeding order, a saturated, short fatty acid (myristic acid) was integrated in the lipid membrane of the g-MSGVs better than the unsaturated oleic and myristoleic acids.

Since both kinds, saturated and unsaturated fatty acids, were able to induce G&D, it is probable that their release from the g- $M_0$ SGVs was different. Lately, a study using free-flow electrophoresis took advantage of the charge on deprotonated oleic acid (**7**), oleate, to show that feeding small unilamellar POPC vesicles (diameter 70 nm) with this acid led to the formation of two populations of vesicles, oleate-poor vesicles and oleate-rich vesicles (Pereira de Souza et al., 2015). Considering the fact that the same phenomena typical for G&D (budding, pearling, evagination, etc.) have been observed on our A type first-generation g- $M_0$ SGVs (Figures 3B and S8–S13) and regarding our results from first, second, and third generation g- $M_{1-3}$ SGVs, it is highly likely that a similar lipid exchange was occurring on our supported membranes. We have observed that more **8** was incorporated in the g-MSGV membranes than **7**, whereas the amount of phospholipid released in the HS by the feeding was very similar (Figures 4F, 4G, and 5). Thus, g- $M_0$ SGVs made of POPC and fed with **7** would produce oleate-poor vesicles, viz. the g- $M_1$ SGVs, and oleate-rich vesicles and aggregates  $D_1$ (GV + LA). Furthermore, this phenomenon would also occur when A type g- $M_0$ SGVs were fed with myristoleic acid (**9**) (Figures 4G and 5 and Table 1). However, using a saturated fatty acid such as **8** would generate membranes that were more symmetrically blended over mothers and daughters (Figures 4E and 5). Interestingly, “hybrid protocells” made of these two types of amphiphiles (phospholipids and fatty acids) showed good properties of stability and permeability (Jin et al., 2018) but they also grew faster than pure fatty acid vesicles (Budín and Szostak, 2011). Our results suggest that the lipid exchange occurring on free vesicles during a G&D process is similar to the one occurring on g-MSGVs and that saturated fatty acids are the privileged amphiphilic feeding material to generate from phospholipid vesicles these more complex, more blended, thus potentially more competitive protocells (Lancet et al., 2018, 2019).

### Conclusion and Perspectives

This optimized methodology for the feeding of glass microsphere-supported giant vesicles is a convenient general tool for the observation and the understanding of the growth and division process over several feeding rounds (generations) in a more controlled analytical way than what was possible before. The method has the potential of providing experimental data for simulation studies on compositional replication in a hypothetical “lipid world” (Kahana and Lancet, 2019; Lancet et al., 2018, 2019; Segre et al., 2000). It could also be applied to other amphiphiles and possibly tested on more artificial coatings than natural phospholipids. In the context of self-evolving compartments, the possibility of generating supported vesicles being composed of mixtures of amphiphiles opens strong perspectives for the study of vesicles that are obtained under so-called prebiotic conditions (Alberstsen et al., Albertsen et al., 2014; Altamura et al., 2020; Fayolle et al., 2017; Fiore et al., 2017; Fiore and Buchet, 2020; Monnard and Deamer, 2003). In this perspective, we can now go on and test how the newly acquired fatty acids could be chemically fixed so as to enrich the compositional complexity of future generations in a more persistent way (Szostak et al., 2001).

### Limitations of the Study

Glass microsphere supported giant vesicles (g-MSGVs, mothers) were used as model protocells to monitor and study growth and division processes of phospholipidic membrane bilayers upon consecutive feedings with fatty acids. The use of g-MSGVs has shown a few limitations and more experiments are required to fully understand their potentiality in origin of life studies. Saturated fatty acids longer than fourteen carbon atoms cannot be used as feeding material, however short saturated chains are more plausibly prebiotic. Time-lapse monitoring of g-MSGVs or DGVs (daughters) was not possible probably due to the technical limitation set by our equipment.

### Resource Availability

#### Lead Contact

Further information and requests for resources should be directed to and will be fulfilled by the Lead Contact, Michele Fiore ([michele.fiore@univ-lyon1.fr](mailto:michele.fiore@univ-lyon1.fr)).

### Materials Availability

This study did generate two new unique compounds  $\omega$ -(dansyl)laurinyl derivative **11** and  $\delta$ -(isopropanylidene)tryptophanyl derivative **12** (Figures S16–S22). Their chemical synthesis and characterization are described in [Supplementary Information](#), and there is no restriction for availability.

### Data and Code Availability

In this study, we have not used any unpublished custom code, software, or algorithm that is central to supporting the main claims of the paper.

## METHODS

All methods can be found in the accompanying [Transparent Methods supplemental file](#).

## SUPPLEMENTAL INFORMATION

Supplemental Information can be found online at <https://doi.org/10.1016/j.isci.2020.101677>.

## ACKNOWLEDGMENTS

M.F. wishes to dedicate this work to the memory of his beloved daughter Océane. The authors are thankful to Laura Faccin and Quentin Da Silva for their contribution in performing preliminary growth and division experiments on A type g-MSVGs. Prof. Agnès Girard-Egrot is gratefully acknowledged for her support in using the microscope facility at GEMBAS–ICMBS. The authors wish to thank Veronica La Padula of the Center Technologique des Microstructures (CTμ) of the University Claude Bernard Lyon 1 for helping in confocal laser scanning microscopy experiments on A+ type g-M<sub>0</sub>SGVs. M.F. wishes to thank professors S. Piotto (University of Salerno) and F. Rossi (University of Siena) for giving him the opportunity to present the preliminary results of this research at the congress third International Conference on Bio and Nanomaterials September 29–October 3, 2019 | MSC cruise, Mediterranean Sea. Prof. Stefano Tonzani is gratefully acknowledged for the invitation to submit this research to iScience. Funding: Volkswagen Foundation “Molecular Life,” Az 92 850.

## AUTHOR CONTRIBUTIONS

A.L. and M.F. performed all G&D experiments, HPLC analyses, Stewart assays, and microscopic observations. D.F. and M.F. synthesized compounds **11** and **12**. M.F. conceived the project, supervised the study, and wrote the first drafts of the manuscript and Electronic [Supplementary Information](#) and assembled the last version of the manuscript. P.S. supervised the study and revised several versions of the draft manuscript. All the authors reviewed and agreed upon the submitted version of the manuscript.

## DECLARATION OF INTERESTS

Authors declare no competing interests.

Received: May 18, 2020

Revised: September 21, 2020

Accepted: October 9, 2020

Published: November 20, 2020

## REFERENCES

- Albertsen, A.N., Maurer, S.E., Nielsen, K.A., and Monnard, P.-A. (2014). Transmission of photo-catalytic function in a self-replicating chemical system: in situ amphiphile production over two protocell generations. *Chem. Commun.* **50**, 8989–8992.
- Altamura, E., Comte, A., D’Onofrio, A., Roussillon, C., Fayolle, D., Buchet, R., Mavelli, F., Stano, P., Fiore, M., and Strazewski, P. (2020). Racemic phospholipids for origin of life studies. *Symmetry* **12**, 1108.
- Berclaz, N., Blöchliger, E., Müller, M., and Luisi, P.L. (2001a). Matrix effect of vesicle formation as investigated by cryotransmission electron microscopy. *J. Phys. Chem. B* **105**, 1065–1071.
- Berclaz, N., Müller, M., Walde, P., and Luisi, P.L. (2001b). Growth and transformation of vesicles studied by ferritin labeling and cryotransmission electron microscopy. *J. Phys. Chem. B* **105**, 1056–1064.
- Bligh, E.G., and Dyer, W.J. (1959). A rapid method of total lipid extraction and purification. *Can. J. Biochem. Physiol.* **37**, 911–917.
- Budin, I., Debnath, A., and Szostak, J.W. (2012). Concentration-Driven growth of model protocell membranes. *J. Am. Chem. Soc.* **134**, 20812–20819.
- Budin, I., and Szostak, J.W. (2011). Physical effects underlying the transition from primitive to modern cell membranes. *Proc. Natl. Acad. Sci. U S A* **108**, 5249–5254.
- Cape, J.L., Monnard, P.-A., and Boncella, J.M. (2011). Prebiotically relevant mixed fatty acid vesicles support anionic solute encapsulation and

- photochemically catalyzed trans-membrane charge transport. *Chem. Sci.* **2**, 661.
- Chen, I.A. (2004). The emergence of competition between model protocells. *Science* **305**, 1474–1476.
- Fayolle, D., Altamura, E., D'Onofrio, A., Madanamothoo, W., Fenet, B., Mavelli, F., Buchet, R., Stano, P., Fiore, M., and Strazewski, P. (2017). Crude phosphorylation mixtures containing racemic lipid amphiphiles self-assemble to give stable primitive compartments. *Sci. Rep.* **7**, 18106.
- Fiore, M., and Buchet, R. (2020). Symmetry breaking of phospholipids. *Symmetry* **12**, 1488.
- Fiore, M., Madanamoothoo, W., Berlioz-Barbier, A., Maniti, O., Girard-Egrot, A., Buchet, R., and Strazewski, P. (2017). Giant vesicles from rehydrated crude mixtures containing unexpected mixtures of amphiphiles formed under plausibly prebiotic conditions. *Org. Biomol. Chem.* **15**, 4231–4240.
- Fiore, M., Maniti, O., Girard-Egrot, A., Monnard, P.-A., and Strazewski, P. (2018). Glass microsphere-supported giant vesicles for the observation of self-reproduction of lipid boundaries. *Angew. Chem. Int. Ed.* **57**, 282–286.
- Gopalakrishnan, G., Rouiller, I., Colman, D.R., and Lennox, R.B. (2009). Supported bilayers formed from different phospholipids on spherical silica substrates. *Langmuir* **25**, 5455–5458.
- Hanczyc, M.M., Fujikawa, S., and Szostak, J. (2003). Experimental models of primitive cellular compartments: encapsulation, growth, and division. *Science* **302**, 618–622.
- Hardy, M.D., Yang, J., Selimkhanov, J., Cole, C.M., Tsimring, L.S., and Devaraj, N.K. (2015). Self-reproducing catalyst drives repeated phospholipid synthesis and membrane growth. *Proc. Natl. Acad. Sci. U S A* **112**, 8187–8192.
- Heron, S., Maloumbi, M.-G., Dreux, M., Verette, E., and Tchaplal, A. (2007). Method development for a quantitative analysis performed without any standard using an evaporative light-scattering detector. *J. Chromatogr. A* **1161**, 152–156.
- Jin, L., Kamat, N.P., Jena, S., and Szostak, J.W. (2018). Fatty acid/phospholipid blended membranes: a potential intermediate state in protocellular evolution. *Small* **14**, 1704077.
- Johnson, J.M., Ha, T., Chu, S., and Boxer, S.G. (2002). Early steps of supported bilayer formation probed by single vesicle fluorescence assays. *Biophys. J.* **83**, 3371–3379.
- Kahana, A., and Lancet, D. (2019). Protobioc systems chemistry analyzed by molecular dynamics. *Life* **9**, 38.
- Lancet, D., Zidovetzki, R., and Markovitch, O. (2018). Systems protobiology: origin of life in lipid catalytic networks. *J. R. Soc. Interf.* **15**, 20180159.
- Lancet, D., Segrè, D., and Kahana, A. (2019). Twenty years of “lipid world”: a fertile partnership with David Deamer. *Life (Basel)* **9**, 77.
- Lopez, A., and Fiore, M. (2019). Investigating prebiotic protocells for a comprehensive understanding of the origins of life: a prebiotic systems chemistry perspective. *Life (Basel)* **9**, 49.
- Matsuo, M., Hirata, Y., Kurihara, K., Toyota, T., Miura, T., Suzuki, K., and Sugawara, T. (2020). Environment-sensitive intelligent self-reproducing artificial cell with a modification-active lipo-deoxyribozyme. *Micromachines* **11**, 606.
- Matsuo, M., Kan, Y., Kurihara, K., Jimbo, T., Imai, M., Toyota, T., Hirata, Y., Suzuki, K., and Sugawara, T. (2019). DNA length-dependent division of a giant vesicle-based model protocell. *Sci. Rep.* **9**, 6916.
- Monnard, P.-A., and Deamer, D.W. (2003). Preparation of vesicles from nonphospholipid amphiphiles. *Methods Enzymol.* **372**, 133–151.
- Morigaki, K., and Walde, P. (2002). Giant vesicle formation from oleic acid/sodium oleate on glass surfaces induced by adsorbed hydrocarbon molecules. *Langmuir* **18**, 10509–10511.
- Pereira de Souza, T., Holzer, M., Stano, P., Steiniger, F., May, S., Schubert, R., Fahr, A., and Luisi, P.L. (2015). New insights into the growth and transformation of vesicles: a free-flow electrophoresis study. *J. Phys. Chem. B* **119**, 12212–12223.
- Pignataro, B., Steinem, C., Galla, H.-J., Fuchs, H., and Janshoff, A. (2000). Specific adhesion of vesicles monitored by scanning force microscopy and quartz crystal microbalance. *Biophys. J.* **78**, 487–498.
- Rebaud, S., Maniti, O., and Girard-Egrot, A.P. (2014). Tethered bilayer lipid membranes (tBLMs): interest and applications for biological membrane investigations. *Biochimie* **107**, 135–142.
- Ruiz-Mirazo, K., Briones, C., and de la Escosura, A. (2014). Prebiotic systems chemistry: new perspectives for the origins of life. *Chem. Rev.* **114**, 285–366.
- Schwille, P. (2019). Division in synthetic cells. *Emerg. Top. Life Sci.* **3**, 551–558.
- Segre, D., Ben-Eli, D., and Lancet, D. (2000). Compositional genomes: prebiotic information transfer in mutually catalytic noncovalent assemblies. *Proc. Natl. Acad. Sci. U S A* **97**, 4112–4117.
- Stano, P., and Luisi, P.L. (2010). Achievements and open questions in the self-reproduction of vesicles and synthetic minimal cells. *Chem. Commun.* **46**, 3639.
- Stewart, J.C. (1980). Colorimetric determination of phospholipids with ammonium ferrioxalate. *Anal. Biochem.* **104**, 10–14.
- Szostak, J.W. (2017). The narrow road to the deep past: in search of the chemistry of the origin of life. *Angew. Chem. Int. Ed.* **56**, 11037–11043.
- Szostak, J.W., Bartel, D.P., and Luisi, P.L. (2001). Synthesizing life. *Nature* **409**, 387–390.
- Terasawa, H., Nishimura, K., Suzuki, H., Matsuura, T., and Yomo, T. (2012). Coupling of the fusion and budding of giant phospholipid vesicles containing macromolecules. *Proc. Natl. Acad. Sci. U S A* **109**, 5942–5947.
- Tomita, T., Sugawara, T., and Wakamoto, Y. (2011). Multiplicity of morphological dynamics of giant multilamellar vesicles in regulated nonequilibrium environments. *Langmuir* **27**, 10106–10112.
- Varela, F.G., Maturana, H.R., and Uribe, R. (1974). Autopoiesis: the organization of living systems, its characterization and a model. *Biosystems* **5**, 187–196.
- Walde, P., Cosentino, K., Engel, H., and Stano, P. (2010). Giant vesicles: preparations and applications. *ChemBioChem* **11**, 848–865.
- Walde, P., Wick, R., Fresta, M., Mangone, A., and Luisi, P.L. (1994). Autopoietic self-reproduction of fatty acid vesicles. *J. Am. Chem. Soc.* **116**, 11649–11654.
- Wick, R., Walde, P., and Luisi, P.L. (1995). Light microscopic investigations of the autocatalytic self-reproduction of giant vesicles. *J. Am. Chem. Soc.* **117**, 1435–1436.
- Zhou, Z., Sayer, B.G., Hughes, D.W., Stark, R.E., and Epanand, R.M. (1999). Studies of phospholipid hydration by high-resolution magic-angle spinning nuclear magnetic resonance. *Biophys. J.* **76**, 387–399.
- Zhu, T.F., Adamala, K., Zhang, N., and Szostak, J.W. (2012). Photochemically driven redox chemistry induces protocell membrane pearling and division. *Proc. Natl. Acad. Sci. U S A* **109**, 9828–9832.
- Zhu, T.F., and Szostak, J.W. (2009). Coupled growth and division of model protocell membranes. *J. Am. Chem. Soc.* **131**, 5705–5713.

**iScience, Volume 23**

**Supplemental Information**

**Chemical Analysis of Lipid Boundaries  
after Consecutive Growth and Division  
of Supported Giant Vesicles**

**Augustin Lopez, Dimitri Fayolle, Michele Fiore, and Peter Strazewski**

## Supplementary text and figures

### Transparent Methods

#### Glossary for the experiments

g-MSGVs = **g**lass-**M**icrosphere **S**upported **G**iant **V**esicles ; D(GV+LA)s = **D**ughter (**G**iant **V**esicles + **L**ipid **A**ggregate)s (without glass core inside); HS = **H**osting **S**olution, refers to the suspension of **g-MSGVs** and/or **D(GV+LA)s**, the latter being present after any feeding period. With **feeding solution**, we refer to any fatty acid solution (suspension) containing 50, 25 or 10 mmol L<sup>-1</sup> (mM) in absolute ethanol. This solution was supplemented to the hosting solution during a feeding period. Min = minutes; hrs = hours; BF = bright field. Abbreviations for phospholipids are reported below.

#### Materials

Phospholipids (POPC **1**, 1-palmitoyl-2-oleoyl-*sn*-glycero-3-phosphocholine); POPA, (**2**, 1-palmitoyl-2-oleoyl-*sn*-glycero-3-phosphate); DOPC, (**3**, 1,2-dioleoyl-*sn*-glycero-3-phosphocholine); DOPA, (**4**, 1,2-dioleoyl-*sn*-glycero-3-phosphate), biotinylated phospholipid DSPE-PEG-2000-Biotin (**5**, 1,2-distearoyl-*sn*-glycero-3-phosphoethanolamine-*N*-[biotinyl (polyethylene glycol)-2000]) and DOPE-Rh (**6**, 1,2-dioleoyl-*sn*-glycero-3-phosphoethanolamine-*N*-lissamine rhodamine B sulfonyl ammonium salt) were purchased from Avanti Lipids Inc. (Alabaster, Alabama, USA). Chloroform, ethanol and HPLC solvents were purchased from Fisher Scientific (LC/MS grade). Monodisperse glass beads were obtained from Bangs Laboratories Inc., Indiana, USA (non-functionalized silica-microspheres of 5.0 ± 0.2 µm diameter).

The fatty acids were analyzed by reversed phase-HPLC (Shimadzu LC20) through a reversed phase C4 column (100 x 2.1 mm, 3 µm, 300 Å, Agilent AdvanceBio RP-mAb) and detected by a laser-driven evaporative light scattering detector (ELSD, Sedere, Sedex 90LT) operating at 40 °C. A linear binary gradient of CH<sub>3</sub>CN (0.1 % formic acid) in H<sub>2</sub>O (0.1 % formic acid) was used as the eluant.

NMR spectra were recorded in CDCl<sub>3</sub> on a Bruker Avance 300 spectrometer at 300 MHz for <sup>1</sup>H and 75 MHz for <sup>13</sup>C and on a Bruker Avance 400 at 400 MHz for <sup>1</sup>H and 100 MHz for <sup>13</sup>C. Chemical shifts of solvents (CDCl<sub>3</sub>: δ<sub>H</sub>=7.26 and δ<sub>C</sub>=77.23 ppm) served as internal references. Signal shapes and multiplicities are abbreviated as br (broad), s (singlet), d (doublet), t (triplet), q (quartet), quint (quintet) and m (multiplet). Where possible, a scalar coupling constant J is given in Hertz (Hz).

#### Microscopy procedures

For microscopy procedures (MP) two different models of microscopes were used and included the preparation of the samples before the analysis with the use of solutions of Nile Red® at different stock concentrations (15 µM and 1 mM). In particular, the microscopy procedure A (MPA) was used to visualize the non-fluorescent glass-supported giant vesicles (g-MSGVs coated with A-E type membranes) and the growth and detachment (G&D) processes that were carried out with them. The microscopy procedure B (MPB) was used to visualize the fluorescent DOPE-Rh-labeled g-MSGVs (A<sup>+</sup> type coating) and the feeding experiments carried out with them. Micrographs were depicted without any graphical treatment and the image size was adjusted respecting the x/y pixel proportions. Feeding and G&D experiments were supported by control experiments that were carried out independently.

## Microscopy

### Microscopy procedure A (MPA).

Epifluorescence microscopy was carried out on a Carl Zeiss inverted microscope Observer Z1 equipped with a 20x, 50x and 100x oil immersion objectives and AxioCam recording. To visualize the g-MSGVs without fluorescent probes, they were stained with solutions of 1 mM or 15  $\mu$ M Nile Red<sup>®</sup> in ethanol corresponding to maximally one fifth of the sample volume, unless stated otherwise. In order to visualize the vesicles, a drop of the host solution (20-50  $\mu$ L HS) was mixed with some of the Nile Red<sup>®</sup> stock solution and directly placed on the slide. A spacer was used between microscope cover slip and slide in all samples containing microspheres, to give them sufficient space.

### Microscopy procedure B (MPB).

As for MPA, a spacer was used between microscope cover slip and slide in all samples containing microspheres, to give them sufficient space. g-MSGVs and D(GV+LA)s were visualized by confocal laser scanning fluorescence microscopy using a Carl-Zeiss inverted microscope LSM 800.

## Preparation of glass microsphere-supported phospholipid giant vesicles (g-MSGVs) (Fig. 2A)

### Step 1. Sample preparation and coating with avidin

This procedure was adapted from Lennox and co-workers (25) and Albertsen et al. (22). According to the technical data provided by Bangs Laboratories, each sample was prepared by using  $9 \cdot 10^5$  glass microspheres suspended in 20.76  $\mu$ L of storage buffer. To prepare the samples, this volume of storage buffer was diluted in 1980  $\mu$ L of 50 mM bicine at pH 8.2 (buffer solution), vortexed for one minute and then centrifuged for 5 min. The supernatant was removed and the microsphere pellet was redispersed in 800  $\mu$ L of buffer, to which 200  $\mu$ L of 0.1 mg/mL avidin from egg white (purchased from Sigma Aldrich, France) solution was added. The dispersion was vortexed for one minute and left at 25 °C for 4 h then at 4° C overnight. To remove the excess of avidin from the dispersion, the glass microspheres were washed 3 times (vortexed 1 min, centrifuged for 5 min at 15,000 rpm, the old supernatant is removed and fresh supernatant is added).

### Step 2. Anchoring of biotinylated lipid on glass microspheres

Biotinylated phospholipids (DSPE-PEG-2000-Biotin **5**, Fig. 2) were added to the sample (200  $\mu$ L of a 1 mg/mL chloroformic solution) in order to reach a final concentration of 200  $\mu$ g/mL of lipids. The chloroform was then evaporated with a gentle flow of argon. After evaporation of the chloroform, the sample was suspended in fresh buffer and vortexed (1 min). In order to favor the coating with the bound avidin-biotin the sample was sonicated during 30 min, incubated on a thermoshaker (45 min at 900 rpm, 25°C), sonicated during 5 additional minutes and eventually vortexed for 1 min. Finally, the glass microspheres were washed 5 times (as indicated previously) in order to remove the excess of **5**.

### Step 3. Coating of phospholipid bilayers on the glass microspheres

Phospholipids POPC, POPA, DOPC, and DOPA, (1–4, Fig. 2) dissolved in chloroform (25 mg/mL, chloroform stock solution) were added to the glass microspheres coated with avidin/biotinylated DSPE-PEG (5) to reach a final concentration of phospholipids of 1 mM. In some cases (g-MSGVs A<sup>+</sup> type, Table S1, entry 2) 0.2 % *mol/mol* of a fluorescent phospholipid DOPE-Rh<sup>+</sup> (6) ammonium salt was also added. The samples were dehydrated under a gentle flow of argon to evaporate the chloroform and resuspended in fresh buffer. Then, as described above, the samples were vortexed (1 min), sonicated (30 min), shaken (45 min at 900 rpm, 25°C), sonicated (5 min) and vortexed again (1 min). During these steps, bilayers of phospholipids were formed around the glass microspheres thanks to weak energy interactions around the biotinylated lipids already coated. Eventually, the glass microspheres were washed 20 times (as indicated previously) to remove the unbound lipids in suspension and to obtain a clean suspension containing the supported giant vesicles (g-MSGVs types A-C, Table S1). When the g-MSGVs were prepared from soybean or egg yolk extracts we obtained D and E type g-MSGVs (Table S1), respectively.

### **Growth and division/detachment (G&D) of membranes from glass microsphere-supported phospholipid giant vesicles (g-MSGVs)**

POPC g-M<sub>0</sub>SGVs A and g-M<sub>0</sub>SGVs A<sup>+</sup> (Table S1) were used to test the stability of the membrane by performing G&D experiments using oleic acid (7) as feeding material. Control experiments were carried out independently using an ethanolic feeding solution that did not contain any fatty acid (Table S1, entry 7). In these “-FA” control experiments we did not observe the formation of any DGVs by epifluorescence microscopy: this cannot exclude the presence of micelles or vesicles smaller than 0.5 μm.

#### **Phase 1. Experimental setup**

The feeding processes for all types of g-MSGVs used were set up as previously described and adapted from Fiore *et al.*, 2018 (24). A general method consists in the use of a sample containing a suspension of g-MSGVs (A-C type membranes, Table S1) into 1 mL of 50 mM Bicine, pH 8.2 fed under magnetic stirring with 10 mM solutions of fatty acids (7-12, Fig. 2) solubilized in pure ethanol. The feeding rate was set to 33 μL/h during 3 hours in order to reach a final concentration of fatty acid of 1 mM, since the ethanol evaporates during the experiment. We observed that, at this concentration, the formation of aggregates was avoided but G&D was still induced. This procedure was validated for oleic, myristic and myristoleic acids (7-9) without any issue and each experiment was performed in triplicate. However, palmitic acid (10) produced floating precipitates at all tested stock concentrations and synthetic compounds 11 and 12 showed a precipitation at any concentrations above 0.2 mM in the HS.

#### **Phase 2. Monitoring G&D from g-MSGVs**

The G&D process was monitored thanks to aliquots taken at different times: every 15 minutes for the first hour, then every half-hour for a total feeding time of three hours. The swab of 10 μL was added to 30 μL of 50 mM Bicine pH 8.2 and 10 μL of 15 μM Nile Red<sup>®</sup> in absolute ethanol. The micrographs were recorded with an Observer Z1 inverted microscope equipped with a 50x or a 100x oil-immersion objective and AxioCam CCD detector (see MPA). Moreover, g-MSGVs containing 0.2% DOPE-Rh (6, g-MSGVs coated with A<sup>+</sup> type membranes, Table S1, entry 2) were submitted to a G&D process with oleic acid only and visualized by a Carl-Zeiss inverted microscope LSM 800 (see MPB).

### **Phase 3. Recovery of the samples**

After each G&D, the g-MSGVs were separated from the host solution (HS) by centrifugation. Thus, the samples were vortexed and subsequently centrifuged (3 min at 15,000 rpm) four times. After 4 vortex-centrifugation cycles, the supernatant was removed and the pellet was suspended with fresh buffer. All the 4 supernatants containing the daughter giant vesicles and lipid aggregates, D(GV+LA)s, were kept for analyses. Then, the resulting g-MSGVs were used as starting material for another round of G&D (after the first or the second G&D) or were kept for chemical analyses. A summary of the procedure is depicted in Fig. 3A.

### **Analyses of the glass microsphere-supported phospholipid-coated giant vesicles (g-MSGVs)**

#### **Lipid extraction from the g-MSGVs and DGVs**

Lipid extraction was performed with the method of Bligh and Dyer (27). The samples containing lipids were suspended in 1.5 mL of water. 5.7 mL of CHCl<sub>3</sub>:MeOH 1:2 (v/v), 1.9 mL of CHCl<sub>3</sub>, and 1.9 mL of H<sub>2</sub>O were successively added to the sample and each addition was followed by 30 seconds of vortex. After a centrifugation of 5 min at 10,000 rpm at room temperature, the chloroform phase containing the lipids was collected.

#### **Phospholipid analysis by Stewart assay**

The phospholipid concentration of D(GV+LA)s and g-MSGVs were assessed by the Stewart assay (29). For each extracted sample, 0.2 mL were diluted 10 times in chloroform. 2 mL of a solution of 100 mM ammonium ferrothiocyanate in water was added and the biphasic mixture was vortexed for 30 seconds. Then, the sample was centrifuged at 15,000 rpm at room temperature for 10 min. The denser chloroform phase containing the lipids complexed with ammonium ferrothiocyanate was collected. The absorbance was measured at 485 nm with a Jasco V-730 UV/visible light spectrophotometer and compared to a calibration curve, in order to read out the concentration of phospholipids in the samples (Fig. S4). The concentration obtained from g-MSGVs coated with POPC:POPA (4:1 molar ratio, g-MSGV B type, Table S1) was  $0.55 \pm 0.03$  mM and was assumed as being the same for all types of g-MSGVs A-C and A<sup>+</sup> (Table 1), since the phospholipids tested were very similar considering their molecular structures. Student tests were applied to assess statistical differences between the different samples.

#### **Fatty acid analysis by HPLC**

For each extracted sample, 0.20 mL of solution was sampled and filtered through a 0.45 μm filter to remove all microspheric glass beads. Then, the samples were dried using a rotary evaporator and continued drying for 1h under vacuum. Finally, the dried lipids were dissolved in MeOH to be analyzed. All fatty acids were quantified according to calibration curves (cf. Figures S5-S7) that were obtained separately under identical chromatographic conditions. These calibration curves were obtained with reference samples of concentrations between 0 and 0.5 mM which were fitted to a power function (28). The Student test was applied to assess statistical differences between the different samples.

**Table S1.** g-M<sub>0</sub>SGVs were fed with different fatty acids and separately characterized for each type of membrane composition, Related to Table 1

Entry	Name and Coating Type	Membrane Composition (molar ratio)	Fed with	Remarks
1	g-M <sub>0</sub> SGV A	POPC	<b>7 – 12</b> or <b>7</b> then <b>8</b> or <b>8</b> then <b>7</b> or <b>7</b> then <b>8</b> then <b>9</b> in consecutive feeding experiments	FAs <b>10</b> , <b>11</b> and <b>12</b> flocculated after few minutes of feeding and were discarded. G-MSGVs A were used to perform three consecutive feeding and G&D cycles, each followed by a complete chemical analysis of g-M <sub>1-3</sub> GVs and D <sub>1-3</sub> (GV+LA)s.
2	g-M <sub>0</sub> SGV A <sup>+</sup>	POPC + 0.2% DOPE Rh ( <b>6</b> )	<b>7</b>	g-M <sub>0</sub> SGVs A <sup>+</sup> were used only for preliminary tests. These tests were performed varying the concentration of <b>7</b> . Fed MSGVs A <sup>+</sup> were used for analysis by confocal fluorescence microscopy.
3	g-M <sub>0</sub> SGV B	POPC/POPA (4:1)	<b>7</b> then <b>8</b>	g-M <sub>0</sub> SGVs B were used to optimize the Stewart assay. g-M <sub>0</sub> SGVs B and C were used for two consecutive G&D feeding experiments. Complete chemical analyses of g-M <sub>1,2</sub> SGVs and D <sub>1,2</sub> (GV+LA)s were performed as well.
4	g-M <sub>0</sub> SGV C	POPC/POPA/DOPC/DOPA (4:1:4:1)	<b>7</b> then <b>8</b>	As for entry 3.
5	g-M <sub>0</sub> SGV D	Soybean extract	<b>7</b>	Chemical analysis was not carried out.
6	g-M <sub>0</sub> SGV E	Egg yolk	<b>7</b>	Chemical analysis was not carried out.
7	g-M <sub>0</sub> SGV A	POPC	Ethanol	Control experiment

**Table S2.** Analysis of the composition of phospholipids for B type g-M<sub>0</sub>SGVs and the composition of avidin for all types of g-M<sub>0</sub>SGVs, Related to Table 1

Concentration of phospholipids coated on g-M <sub>0</sub> SGVs (mM)	0.55 ± 0.03
Approximate number of phospholipids coated on g-M <sub>0</sub> SGVs in 1 sample	3.31·10 <sup>17</sup>
Number of M <sub>0</sub> SGVs in 1 analyzed sample	9·10 <sup>5</sup>
Approximate number of phospholipids coated on one g-M <sub>0</sub> SGV (B type)	3.7·10 <sup>11</sup>
Concentration of avidin used to coat the glass microspheres (mM)	3.03·10 <sup>-13</sup>
Maximum number of avidin molecules coated on g-M <sub>0</sub> SGVs in 1 sample	1.82·10 <sup>14</sup>
Maximum number of avidin molecules coated on one g-M <sub>0</sub> SGV (whatever coating type)	2·10 <sup>8</sup>

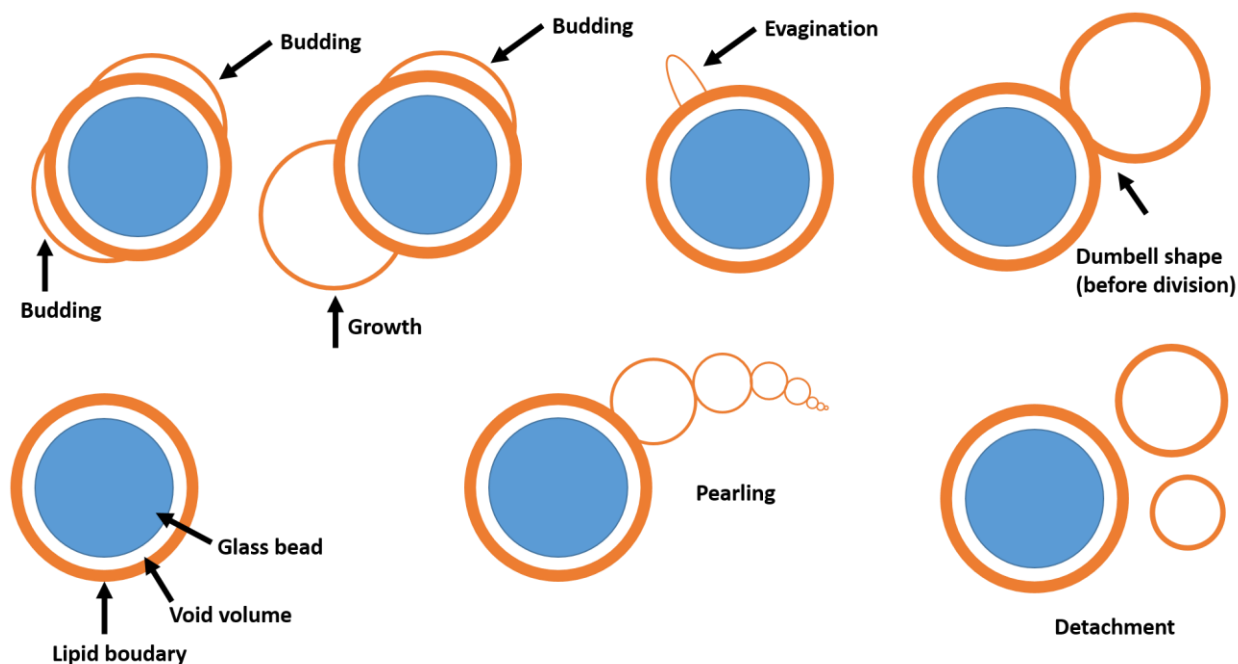


**Figure S1.** Graphical representation of the main phenomena observable during G&D processes (1, 2). Blue filled circles represent the glass microsphere, the orange circles represent the lipid boundaries irrespective of their composition and the composition of the feeding material; Related to Table 1 and Introduction.

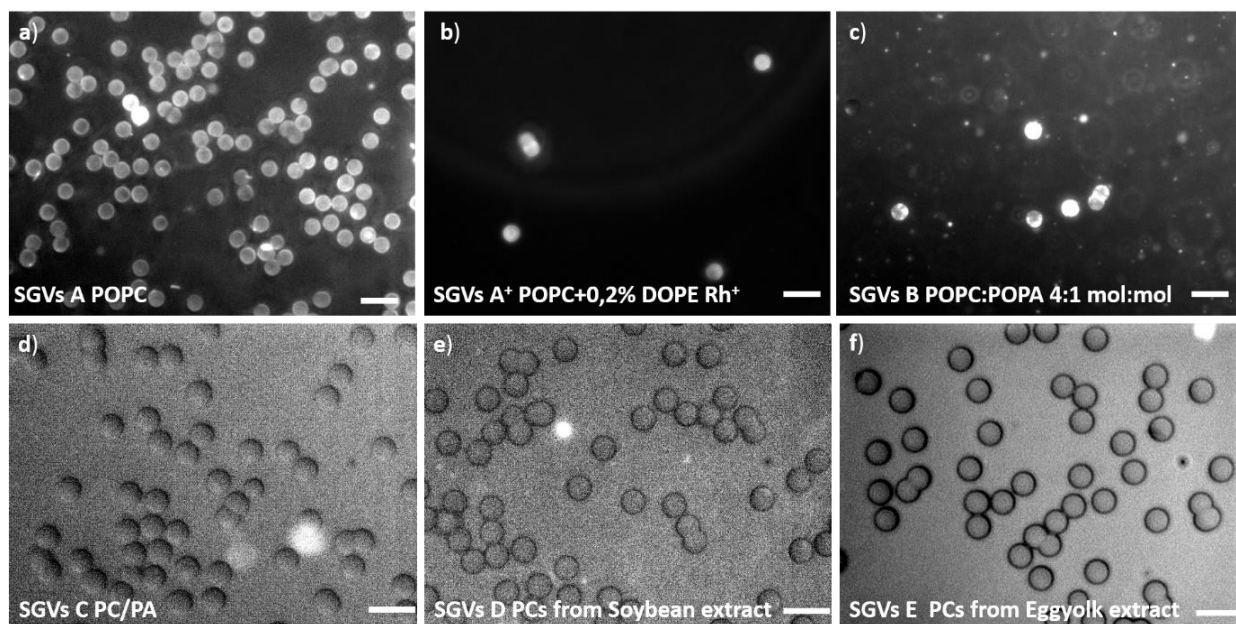


**Figure S2.** Micrographs of g-MSGVs A-E (cf. Table S1). Micrographs a, c (using a 50x lens) and d-f (using a 100x oil immersion lens) were obtained by staining with 0.2 mM Nile Red®; Micrograph b was obtained without staining but the sample contained 0.2 % *mol/mol* of DOPE-Rh (6). All images were obtained using Microscopy Procedure A (MPA). The scale bar is 10 µm for all images. The number of the objects in figure b and c appears lower irrespectively to the total concentration of the g-MSGVs due to different sampling; Related to Table 1 and Introduction.

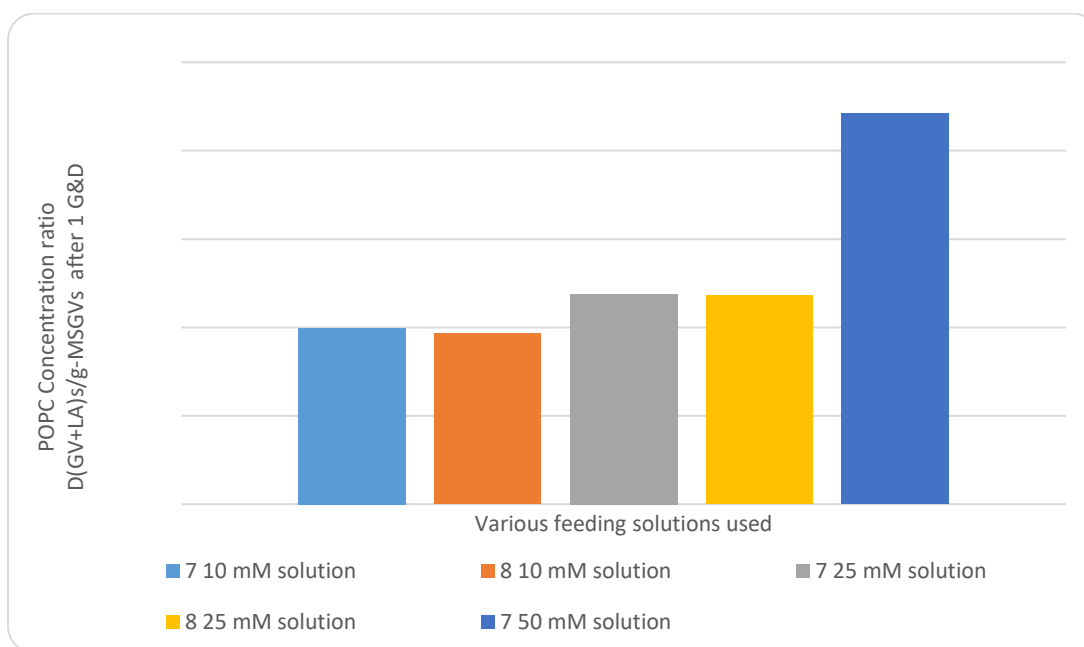


**Figure S3.** Ratio between detached POPC (1) in  $D_1(GV+LA)s$  and supported POPC on g-M<sub>1</sub>GVs after feeding periods with different feeding solutions of oleic acid (7) and myristic acid (8): results from preliminary feeding experiments; Related to Table 1

### Calibration for the quantification analyses

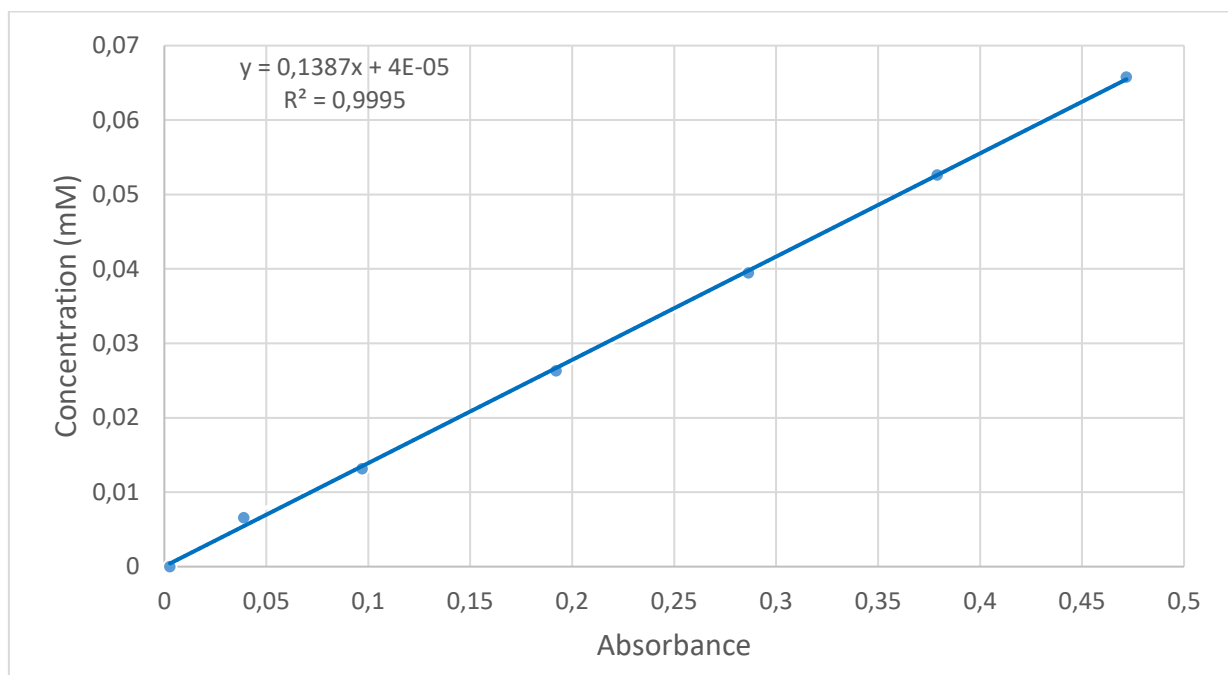


**Figure S4.** Calibration curve to determine the concentrations of phospholipids **1–4** present in the various samples tested. POPC solutions were used as standard for the calibration curve; Related to Tables 1 and S1.

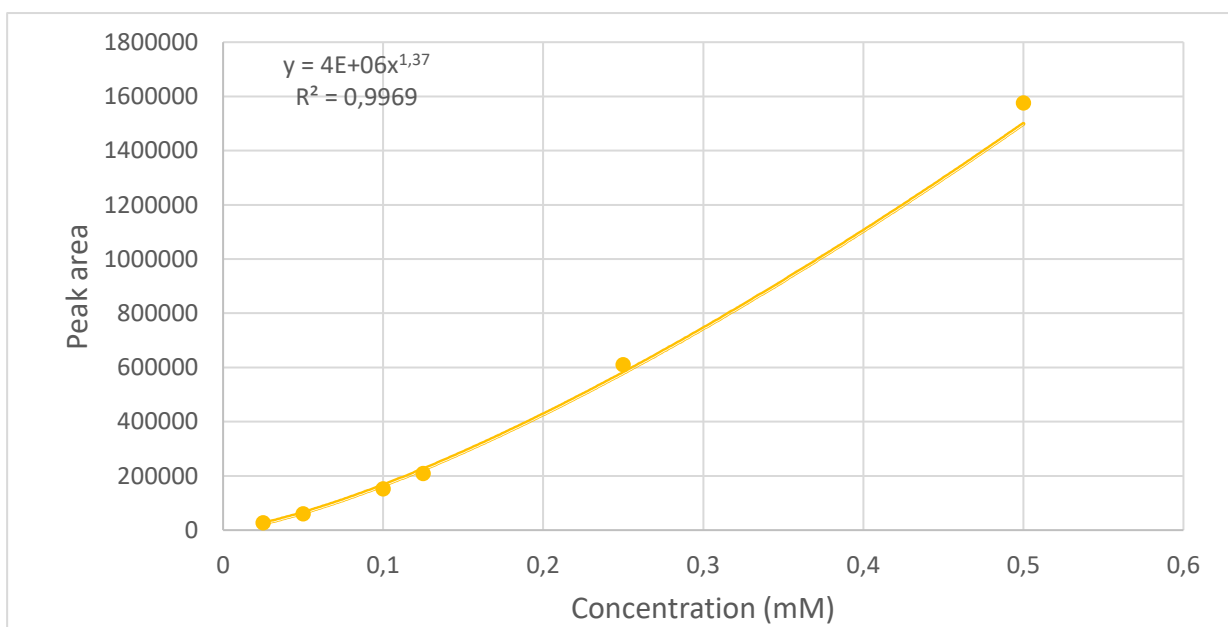


**Figure S5.** Calibration curve (ELSD peak area versus molar concentration) to determine the concentration of oleic acid (**7**) present in the various samples tested. Oleic acid was used as first or second feeding material; Related to Tables 1 and S1.

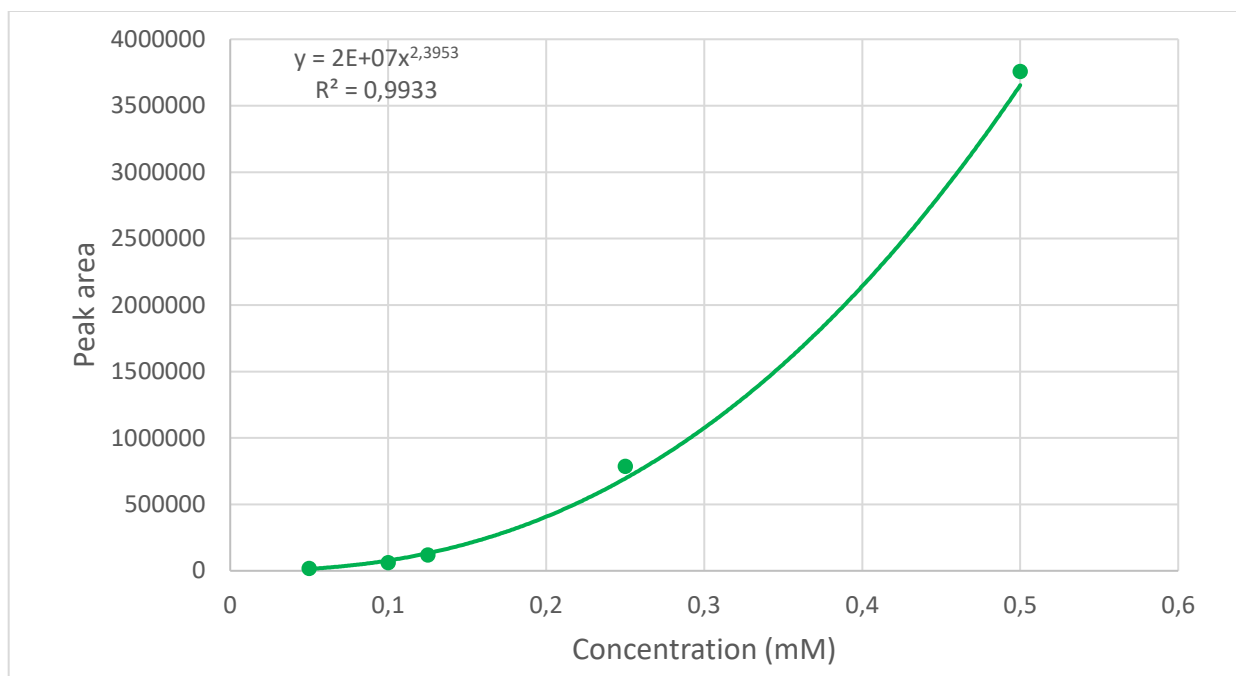


**Figure S6.** Calibration curve (ELSD peak area versus molar concentration) to determine concentration of myristic acid (**8**) present in the various samples tested. Myristic acid was used as first or second feeding material; Related to Tables 1 and S1.

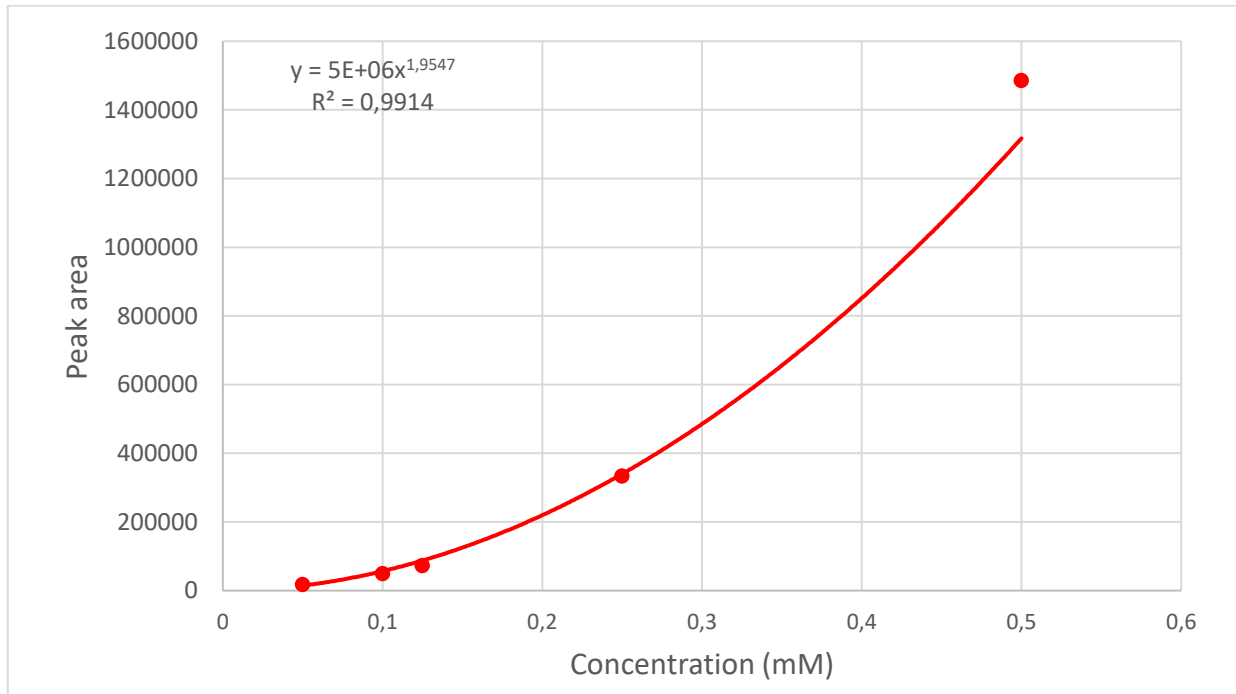


**Figure S7.** Calibration curve (ELSD peak area versus molar concentration) to determine the concentration of myristoleic acid (**9**) present in the various samples tested. Myristoleic acid was used as third feeding material; Related to Tables 1 and S1.

## Microscopic images

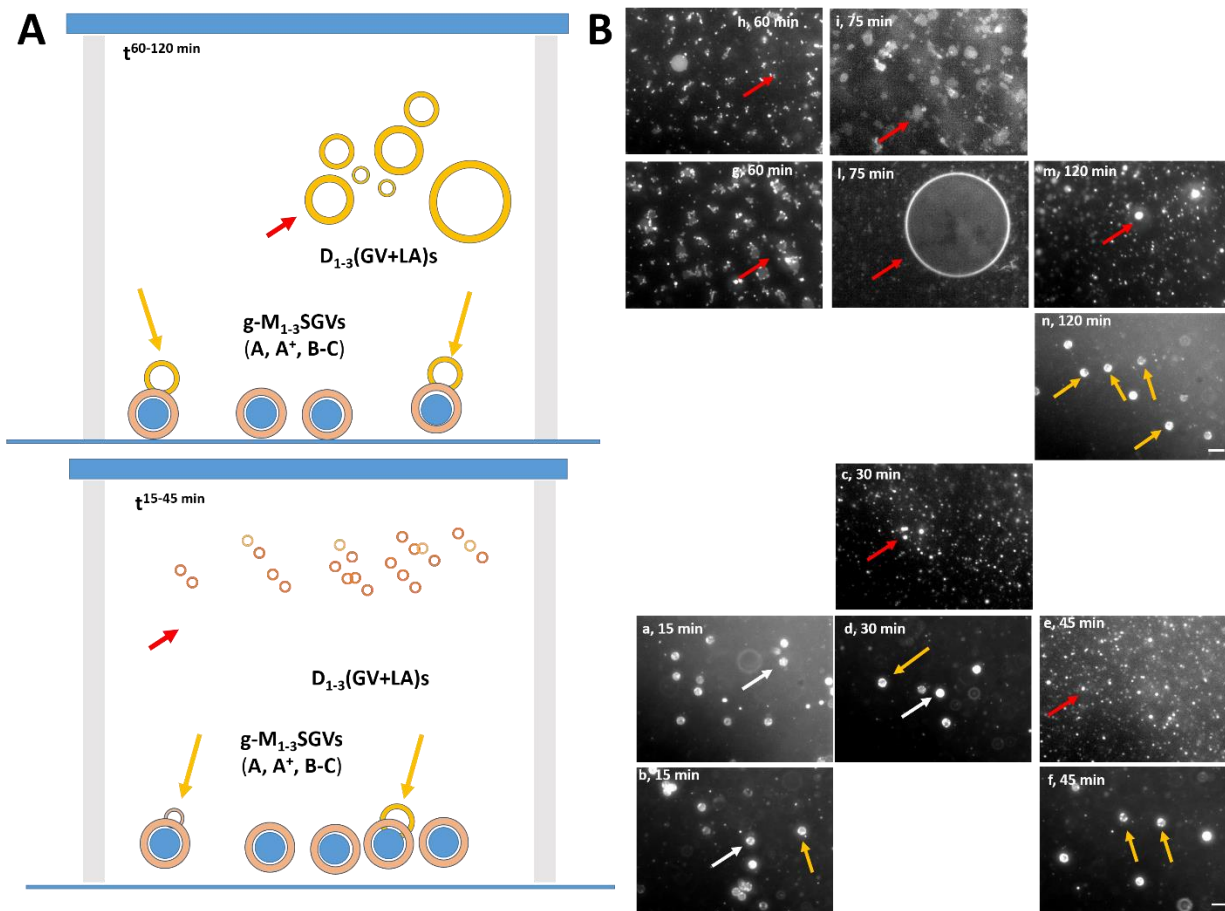


**Figure S8.** Micrographs (MPA) of samples taken over 120 min, that is, between the beginning of the feeding procedure ( $t^{15}$ , pictures **a,b**) and its end ( $t^{120}$ , pictures **m** and **n**) are presented. Feeding ratio was 33  $\mu\text{L}/\text{min}$  and the stock concentration of oleic acid (**7**) was 10 mM as ethanol solution. **A**) Front schematic view of the system slide (in blue)/spacer (in grey)/mother vesicles (blue filled) and daughter vesicles and lipid aggregates (orange/yellow) during microscopic procedures (MPA). Budding, growth and dumbbell shapes are indicated with an orange arrow, newly formed vesicles with a red arrow. The schematic drawing is not in scale. **B**) Pictures: **a,b**) The g-M<sub>1-3</sub>SGVs (A type, Table S1, indicated with a with white arrows) as they appeared in the beginning of the experiment, a little growth of the lipid boundary (indicated with a yellow arrow) began to appear; **c**) New small floating vesicles and lipid aggregates ( $D_1(\text{GV}+\text{LA})\text{s}$ ), indicated with a red arrow) began to appear after 15 minutes feeding; **d**) Swelling (indicated with a yellow arrow) of the lipid coating of the g-M<sub>1</sub>SGVs developed after 30 min. **e**) The number of floating  $D_1(\text{GV}+\text{LA})\text{s}$  increased with increasing feeding time; **f**) Swelling of the lipid coating of the g-M<sub>1</sub>SGVs developed after 45 min, budding and growing are indicated with yellow arrows. **g-l**) Size of floating  $D_1$ GVs was increasing over the course of the G&D experiments, budding phenomena were also visible; **m-n**)  $D_1(\text{GV}+\text{LA})\text{s}$  coexisted with g-M<sub>1</sub>SGVs. Each sample was stained with 0.2 mM Nile Red<sup>®</sup> ( $1/5^{\text{th}}$  of the analyzed volume of hosting solution) before visualization. The scale bar for all micrographs is 10  $\mu\text{m}$ ; Related to Table 1

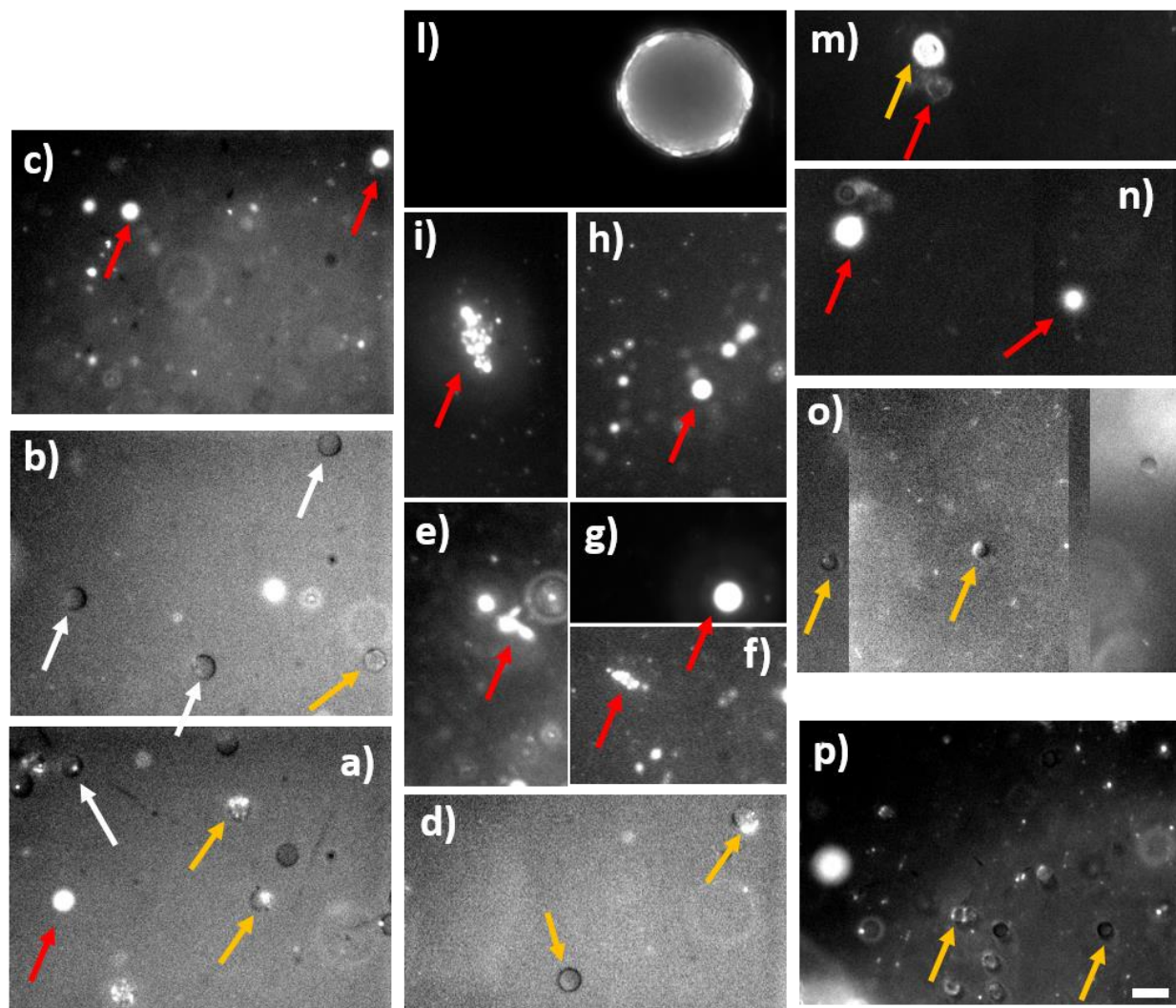


**Figure S9.** Micrographs (MPA) of samples taken over 240 min, that is, between the start of the feeding procedure ( $t^{0-60'}$ , pictures **a-c**) and its end ( $t^{240'}$ , picture **p**). Feeding ratio was 33  $\mu\text{L}/\text{min}$  and the concentration of myristic acid (**8**) was 10 mM as ethanol solution. Pictures: **a,b**) The g-M<sub>1</sub>SGVs (B type, Table S1) type fed with **8**, indicated with a white arrow, began to display budding and growth (indicated with yellow arrows) after 15 minutes of feeding; **c**) New small floating vesicles and lipid aggregates (D<sub>2</sub>(GV+LA)s, indicated with red arrows) began to appear after 15, 45 and 60 minutes of feeding; **d**) Swelling (indicated with a yellow arrow) of the lipid coating of the g-M<sub>2</sub>SGVs developed after 30 min. **a-n**) The number of floating daughter GVVs (D<sub>2</sub>GVs), indicated with a red arrow, increased with increasing feeding time: many floating vesicles started appearing after 90-180 min of feeding (**l**); **o, p**) D<sub>2</sub>(GV+LA)s coexisted with M<sub>2</sub>SGVs. Each sample was stained with 0.2 mM Nile Red<sup>®</sup> (1/5<sup>th</sup> of the analyzed volume of hosting solution) before visualization. The scale bar is 10  $\mu\text{m}$  for all micrographs; Related to Table 1

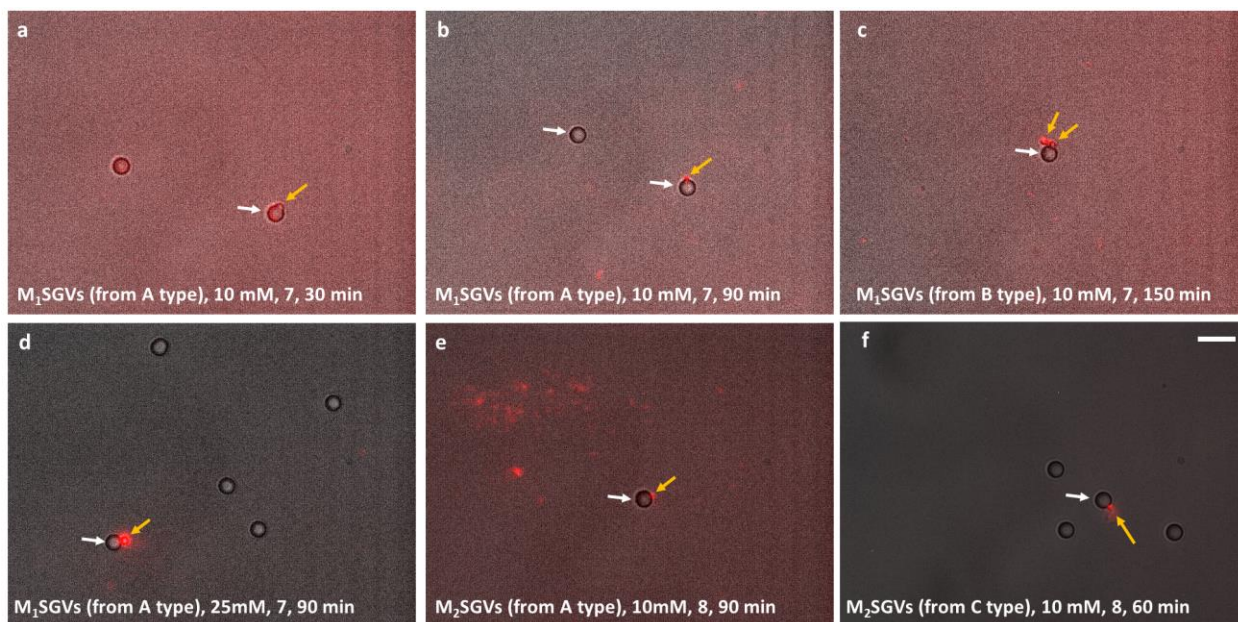


**Figure S10.** Micrographs (MPA) of samples taken over 150 min during different feeding experiments showing budding generated on the lipid boundary of g-MSGVs during the 1<sup>st</sup> and the 2<sup>nd</sup> feeding experiments. Experiments refer to those described in Fig. S8. Feeding ratio was kept at 33 μL/min and the concentration of oleic acid (**7**) and myristic acid (**8**) was 10 or 25 mM as ethanol solution. White arrows indicate the g-MSGVs and the orange arrows indicate budding. Each sample was stained with 3 μM Nile Red® before visualization. Pictures **a-d**, g-M<sub>1</sub>GVs from a 1<sup>st</sup> feeding process, **e-f**, from a 2<sup>nd</sup> feeding process. The scale bar is 10 μm for all micrographs; Related to Table 1

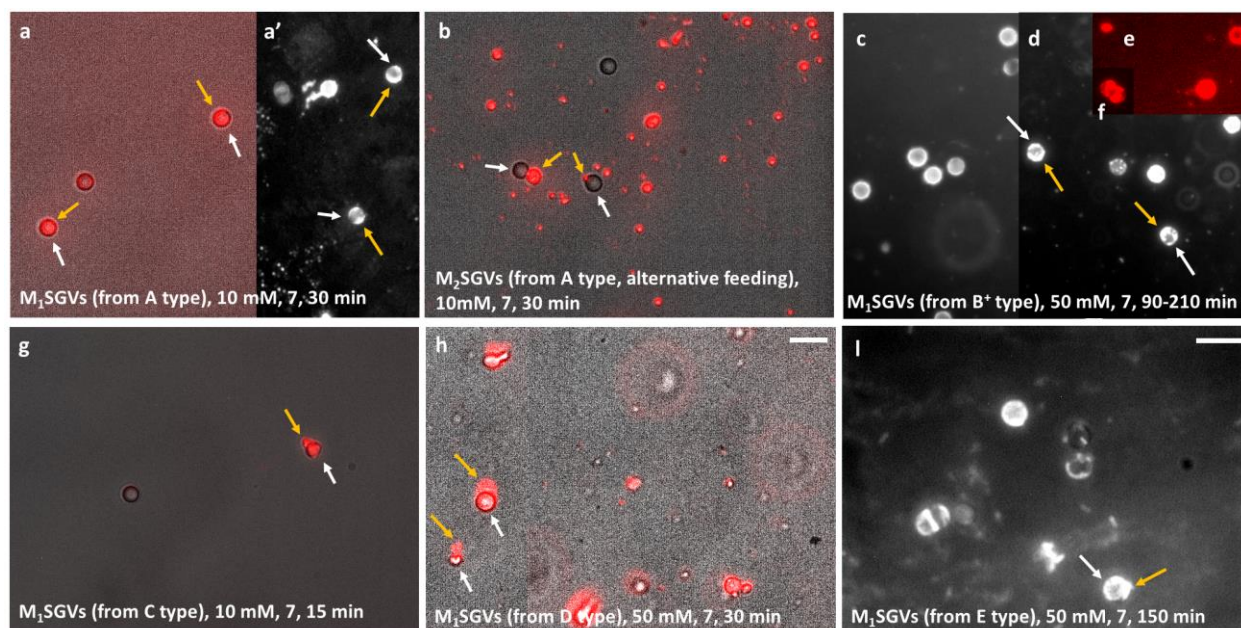


**Figure S11.** Micrographs of samples taken over 210 min during different feeding experiments showing membrane growth generated on the lipid boundary of g-MSGVs during the 1<sup>st</sup> and the 2<sup>nd</sup> feeding experiments. Experiments refer to those described in Fig. S8. The feeding ratio was kept at 33  $\mu$ L/min and the concentration of oleic acid (7) and myristic acid (8) was 10, 25 or 50 mM as ethanol solution. The orange arrows indicate the growth phenomena. Each sample was stained with 3  $\mu$ M Nile Red<sup>®</sup> before visualization. The scale bar is 10  $\mu$ m for all micrographs; Related to Table 1



**Figure S12.** Micrographs (MPA) of samples taken over 120 min during different feeding experiments showing pearling generated on the lipid boundary of SGVs during the 1<sup>st</sup> feeding experiment. Experiments refer to those described in Fig. S8. Feeding ratio was kept at 33 $\mu$ L/min and the concentration of oleic acid (7) was 10 or 25 mM as ethanol solution. Each sample was stained with 3  $\mu$ M Nile Red<sup>®</sup> before visualization. The scale bar is 10  $\mu$ m for all micrographs; Related to Table 1

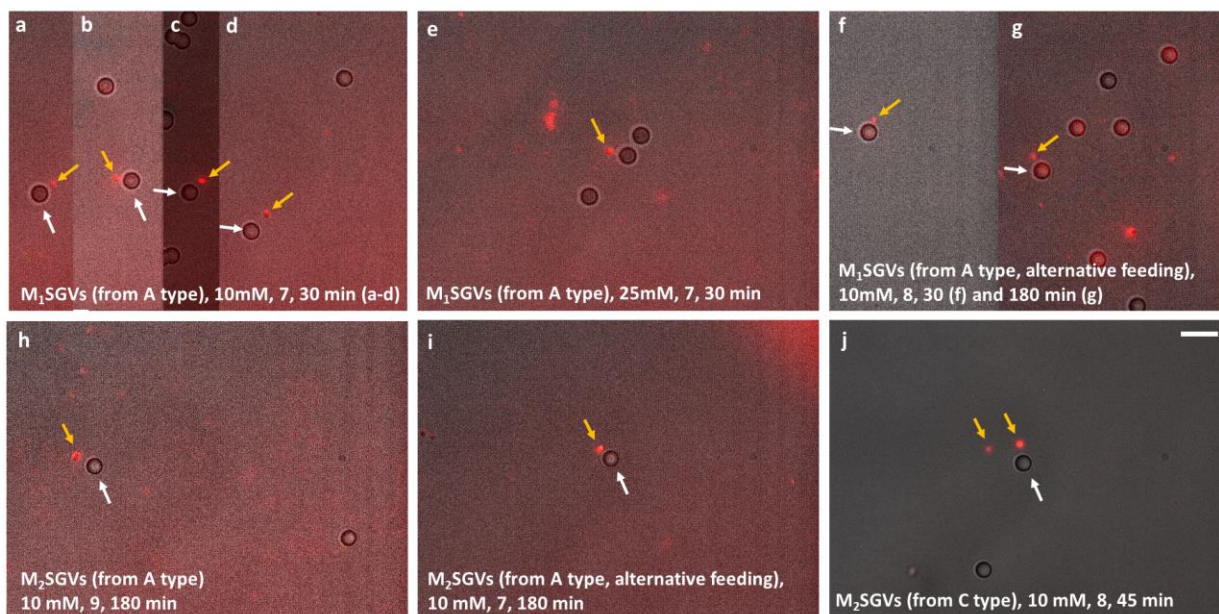


**Figure S13.** Micrographs (MPA) of samples taken over 180 min during different feeding experiments showing division generated on the lipid boundary of SGVs during the 1<sup>st</sup> and 2<sup>nd</sup> feeding experiment. Experiments refer to those described in Fig. S10. The feeding ratio was kept at 33  $\mu$ L/min and the concentration of oleic acid (**7**) was 10 or 25 mM as ethanol solution. Each sample was stained with 3  $\mu$ M Nile Red<sup>®</sup> before visualization. The scale bar is 10  $\mu$ m for all micrographs; Related to Table 1

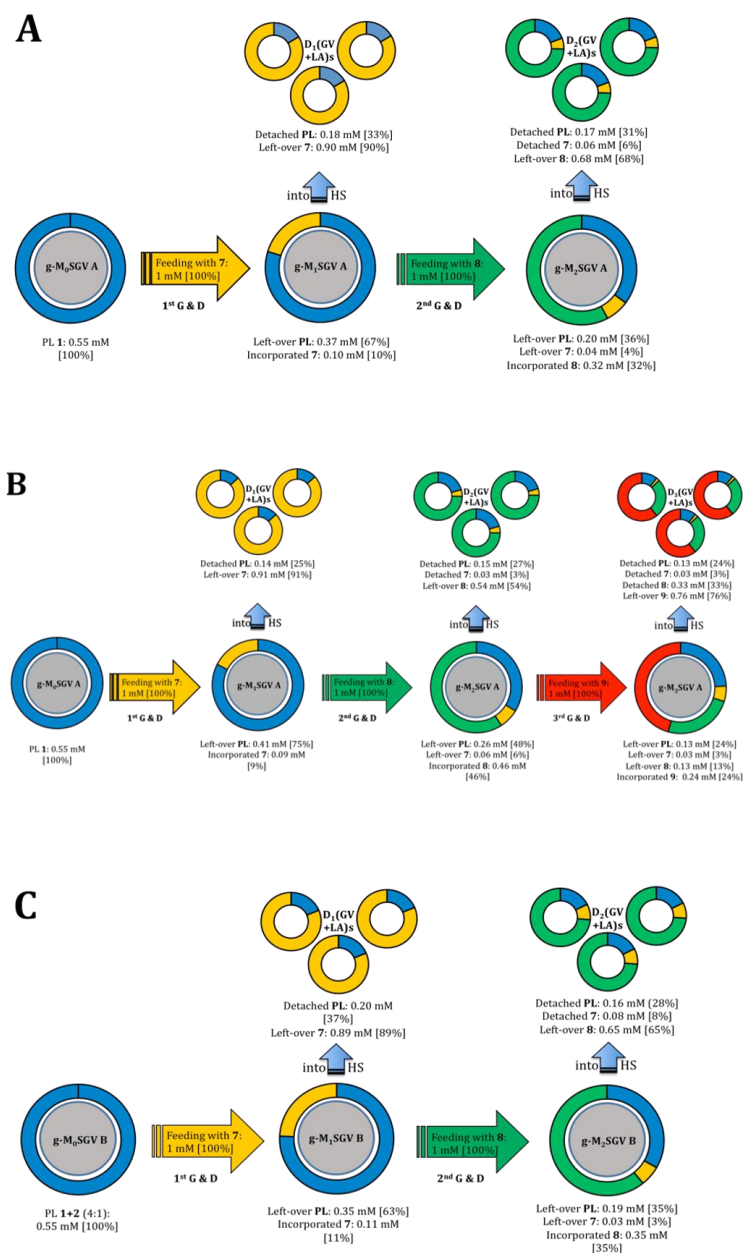


**Figure S14.** Schematic representation of all measured and calculated feeding processes. Concentrations and partition values taken and calculated from Table 1: A) entry 1 (A type coating); B) entry 2 (A type coating) ; C) entry 3 (B type coating); Percentages in square brackets refer to concentration of phospholipids and fatty acids of g- $M_{0-3}$ SGVs and  $D_{1-3}(GV+LA)s$  partitioned over mothers and daughters after each feeding step: [% = concentration of one amphiphile type / total concentration of this amphiphile type]. Total concentration of PL (0.55 mM) corresponds to amount on g- $M_0$ SGVs. Total concentration of each fatty acid 7–9 (1 mM) corresponds to supply during each respective feeding period. Color code in ring charts corresponds to compounds as shown in Fig. 2B and membrane compositions as depicted in Fig. 4 (main manuscript) and used in Figs. S4-S7; related to Figures 4 and 5

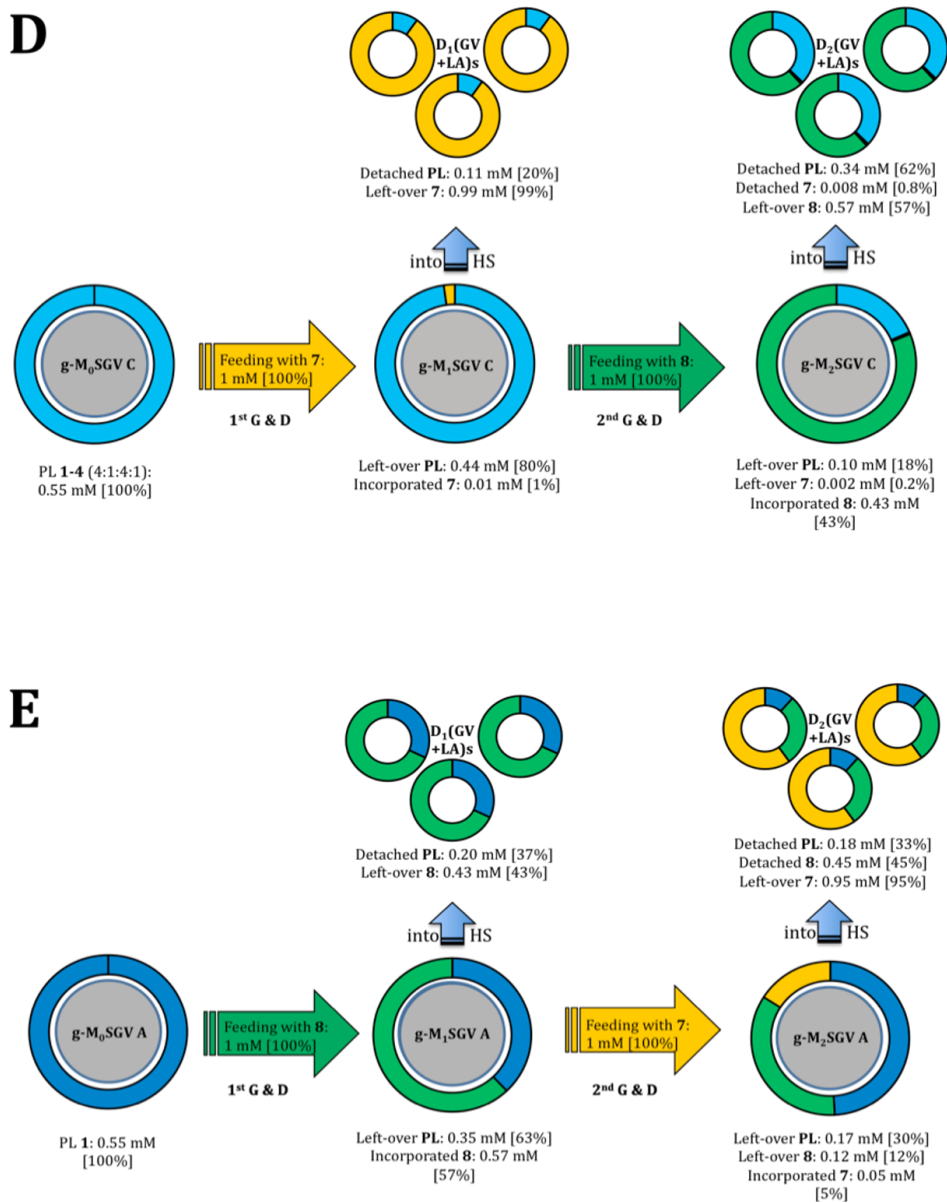
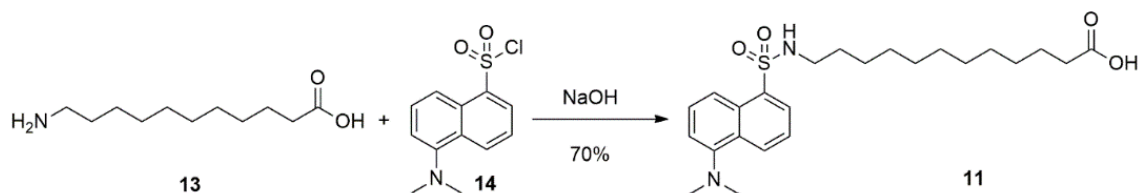
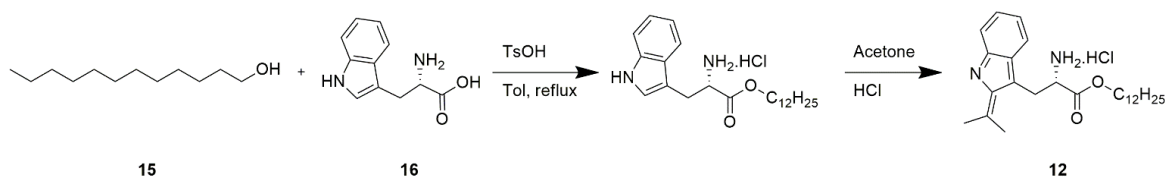


**Figure S15.** Schematic representation of all measured and calculated feeding processes. Concentrations and partition values taken and calculated from Table 1: D) entry 4 (C type coating) ; E) entry 5 (A type coating, inverted feeding order). Percentages in square brackets refer to concentration of phospholipids and fatty acids of g- $M_{0-3}$ SGVs and  $D_{1-3}(GV+LA)s$  partitioned over mothers and daughters after each feeding step: [% = concentration of one amphiphile type / total concentration of this amphiphile type]. Total concentration of PL (0.55 mM) corresponds to amount on g- $M_0$ SGVs. Total concentration of each fatty acid 7–9 (1 mM) corresponds to supply during each respective feeding period. Color code in ring charts corresponds to compounds as shown in Fig. 2B and membrane compositions as depicted in Fig. 4 (main manuscript) and used in Figs. S4-S7; related to Figures 4 and 5

## Synthesis of compounds 11 and 12



**Scheme S1.** Synthesis of compound **11**; related to introduction part and Table 1



**Scheme S2.** Synthesis of compound **12**; related to introduction part and Table 1

## Chemical characterization, NMR and HRMS spectra of compounds 11 and 12

**Compound 11.** 12-aminolauric acid (**13**, 215 mg, 1.06 mmol) and dansyl chloride (**14**, 269 mg, 1.00 mmol) were mixed together with NaOH (40 mg, 1 mmol) in 10 ml of acetone and 4 ml of distilled water. The suspension was stirred at room temperature for 16 hrs. The green-yellow solution was then diluted in water (20 mL) and extracted twice with chloroform (2x15 mL). The reunited organic layers were washed with brine (20 mL), dried over Na<sub>2</sub>SO<sub>4</sub> and the solvent was evaporated under reduced pressure. Purification of the crude extract was performed on a 15 cm silica gel column under isocratic flash chromatography conditions (CHCl<sub>3</sub>) that yielded 313 mg (70 %) of pure **11** as dark yellowish oil. R<sub>f</sub> (CHCl<sub>3</sub>) 0.31; <sup>1</sup>H NMR (CDCl<sub>3</sub>, 300 MHz): δ<sub>H</sub> = 8.65 (d, *J* = 8 Hz, 1H), 8.39 (d, *J* = 8.3 Hz, 1H), 8.26 (d, *J* = 8.5 Hz, 1H), 7.60-7.53 (m, 1H), 3.21-2.85 (m, 8H), 2.35 (t, *J* = 7.4 Hz, 2H); 1.68-1.65 (m, 2H) ppm. <sup>13</sup>C NMR (CDCl<sub>3</sub>, 100 MHz): δ<sub>C</sub> = 179.7, 128.5, 46.6, 34.3, 29.8, 29.5, 29.4, 29.2, 26.6, 24.9 ppm. Exact mass (M+H)<sup>+</sup> calcd. for C<sub>24</sub>H<sub>37</sub>N<sub>2</sub>O<sub>4</sub>S 449.2469 found 449.2459 (2.2 ppm)

**Compound 12.** L-tryptophan (**16**, 10.2 g, 50 mmol), 1-dodecanol (**15**, 11.2 mL, 50 mmol) and *p*-toluenesulfonic acid (11.4 g, 60 mmol) were refluxed in toluene (150 mL) for 3h using a Dean-Stark apparatus. The solvent was then removed, and the resulting brown oil was dissolved in chloroform (150 mL), washed with 10 % aqueous Na<sub>2</sub>CO<sub>3</sub> (3 x 300 mL), brine (300 mL) dried on Na<sub>2</sub>SO<sub>4</sub> and concentrated to dryness. The brown oily residue was then dissolved in acetone containing conc. HCl (5 vol%, 150 mL) at reflux, then cooled down and kept at -20°C overnight to induce crystallization of the hydrochloride salt. The precipitate was recrystallized again from acetone (10 ml) two times (dissolving at 50 °C and precipitating at -20 °C) to yield the title compound as an off-white powder (3.91 g, 17%). <sup>1</sup>H NMR (CDCl<sub>3</sub>, 400 MHz): δ<sub>H</sub> = 7.46 (m, 1H), 7.37 (m, 1H), 7.18-7.11 (m, 1H), 7.08-7.01 (m, 1H), 4.68 (dd, *J* = 11.9, 5.3 Hz, 1H), 4.43-4.28 (m, 2H), 3.44 (dd, *J* = 16, 5.3 Hz, 1H), 3.12 (dd, *J* = 16, 11.9 Hz), 1.91 (s, 3H), 1.83-1.73 (m, 2H), 1.77 (s, 3H), 1.50-1.22 (br, 18H), 0.92-0.86 (m, 3H) ppm. <sup>13</sup>C NMR (CDCl<sub>3</sub>, 100 MHz): δ<sub>C</sub> = 170.1, 138.4, 134.9, 126.9, 123.6, 120.7, 119.1, 112.5, 104.3, 67.8, 58.5, 53.5, 33.1, 30.8, 30.8, 30.7, 30.7, 30.5, 30.4, 29.6, 26.9, 26.3, 26.1, 24.2, 23.8, 23.7, 14.5 ppm. Exact mass (M+H)<sup>+</sup> calcd. for C<sub>26</sub>H<sub>41</sub>N<sub>2</sub>O<sub>2</sub> 413.3163, found 413.3148 (3.5 ppm)

## NMR and MS spectra of compounds 11 and 12

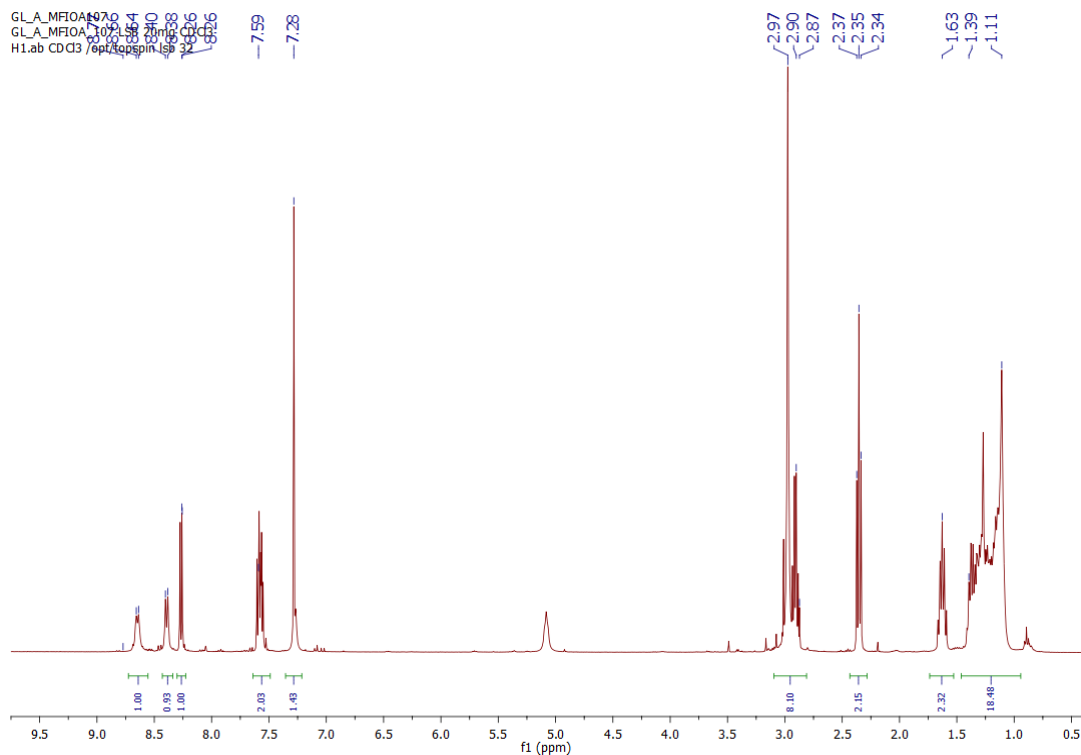


**Figure S16.**  $^1\text{H}$  NMR spectrum ( $\text{CDCl}_3$ , 300MHz) of compound **11**; related to introduction part and Table 1

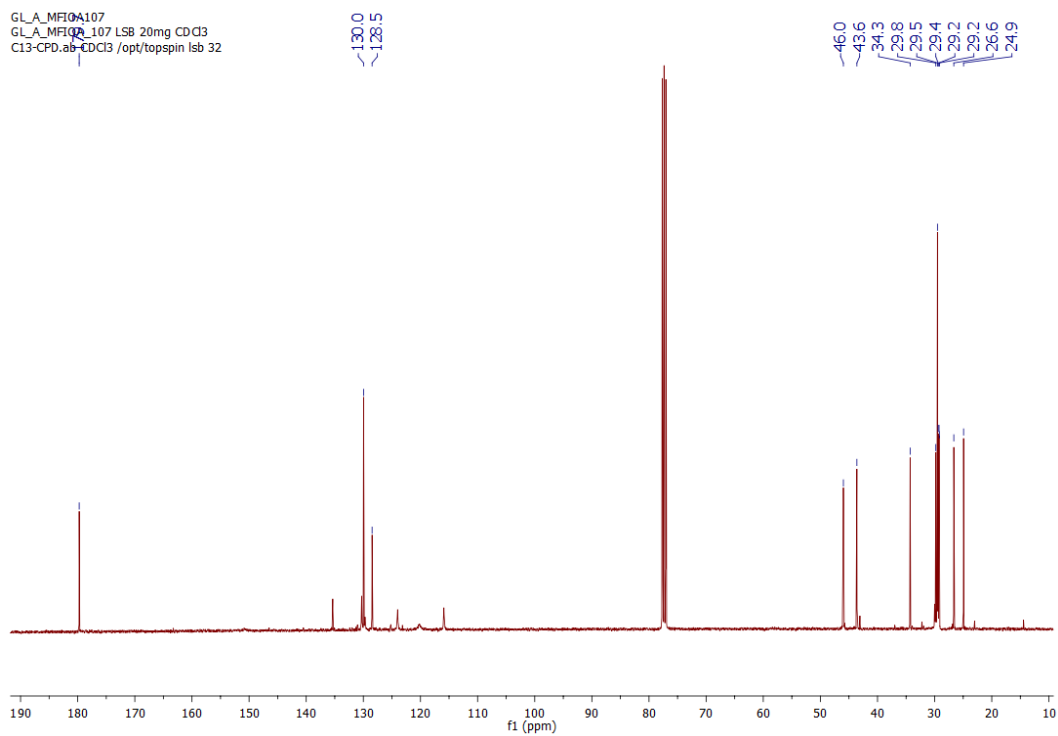


**Figure S17.**  $^{13}\text{C}$  NMR spectrum ( $\text{CDCl}_3$ , 75 MHz) of compound **11**; related to introduction part and Table 1

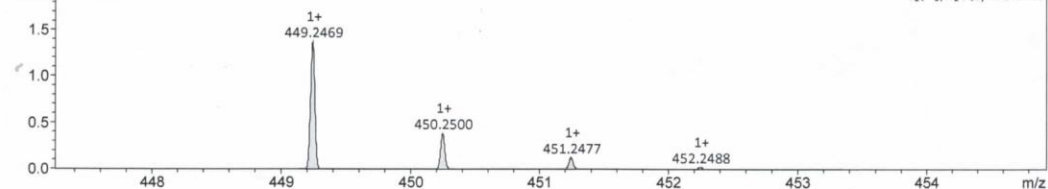
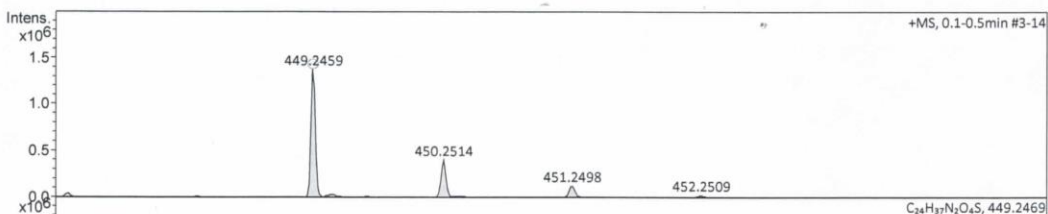
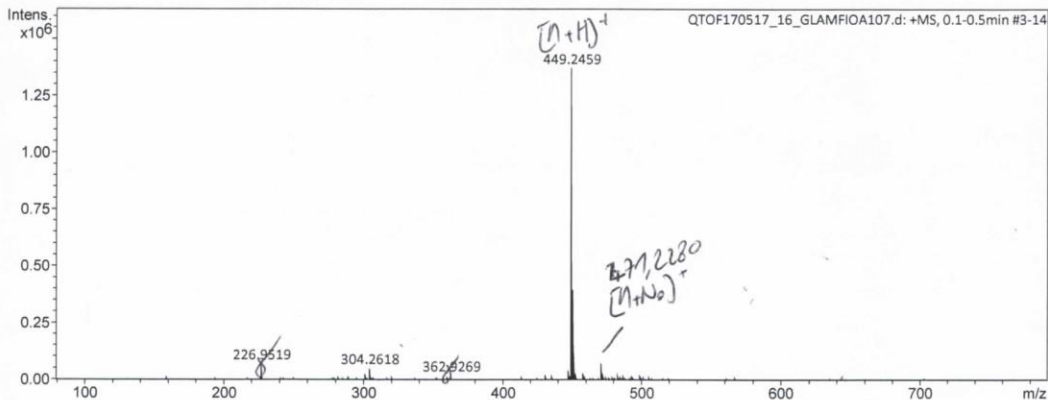
CENTRE COMMUN DE SPECTROMETRIE DE MASSE

**Analysis Info**

Analysis Name QTOF170517\_16\_GLAMFIOA107.d  
 Method 2016\_03\_17\_Infusion\_50-1000\_pos.m  
 Comment  
 Acquisition Date 5/17/2017 3:31:47 PM  
 Instrument / Ser# micrOTOF-Q 228888.10  
 231

**Acquisition Parameter**

Source Type	ESI	Ion Polarity	Positive	Set Nebulizer	0.4 Bar
Focus	Active	Set Capillary	3500 V	Set Dry Heater	200 °C
Scan Begin	50 m/z	Set End Plate Offset	-500 V	Set Dry Gas	4.0 l/min
Scan End	1000 m/z	Set Collision Cell RF	400.0 Vpp	Set Divert Valve	Waste



Meas. m/z	Ion Formula	m/z	err [ppm]	mSigma
449.2459	C <sub>24</sub> H <sub>37</sub> N <sub>2</sub> O <sub>4</sub> S	449.2469	2.2	4.6

**Figure S18.** HRMS spectrum of compound **11**; related to introduction part and Table 1

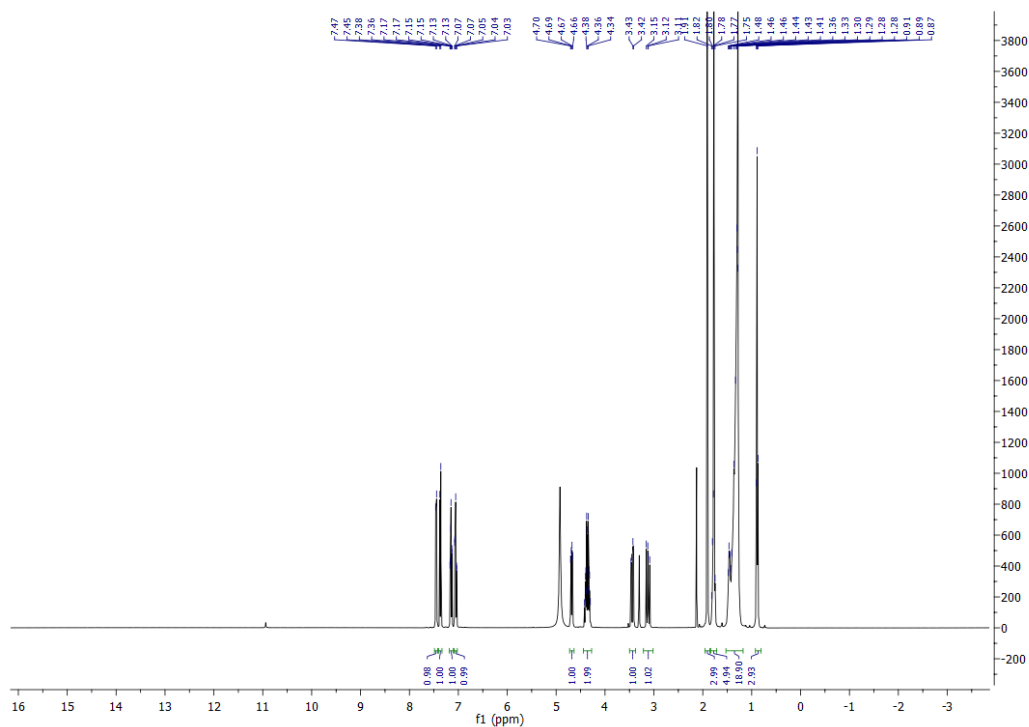


**Figure S19.**  $^1\text{H}$  NMR spectrum ( $\text{CDCl}_3$ , 400MHz) of compound **12**; related to introduction part and Table 1

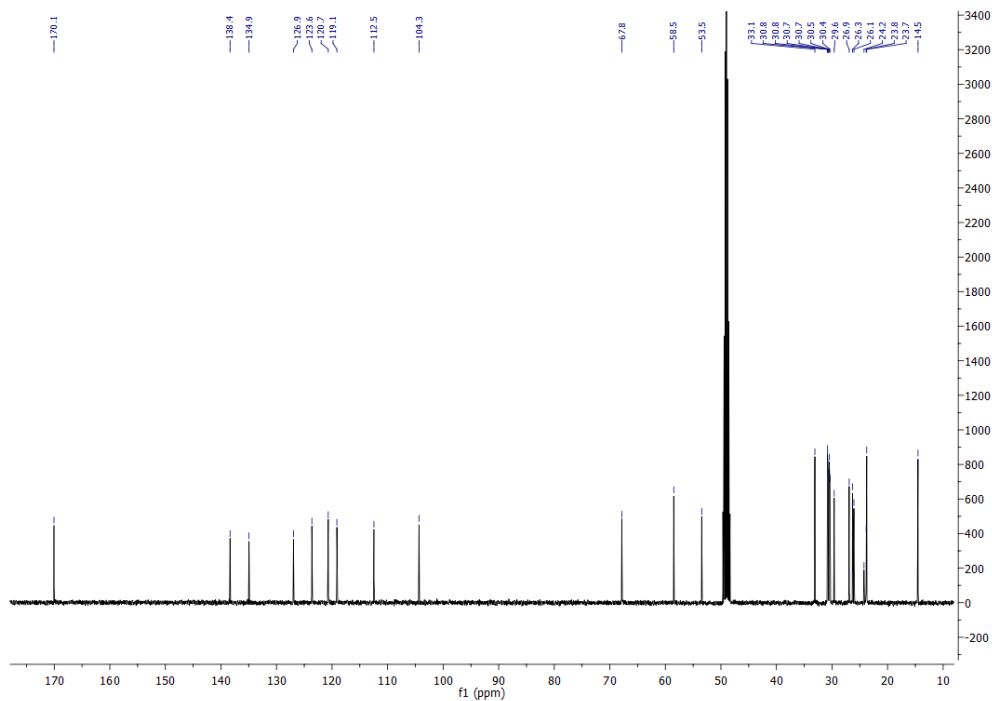


**Figure S20.**  $^{13}\text{C}$  NMR spectrum ( $\text{CDCl}_3$ , 100MHz) of compound **12**; related to introduction part and Table 1

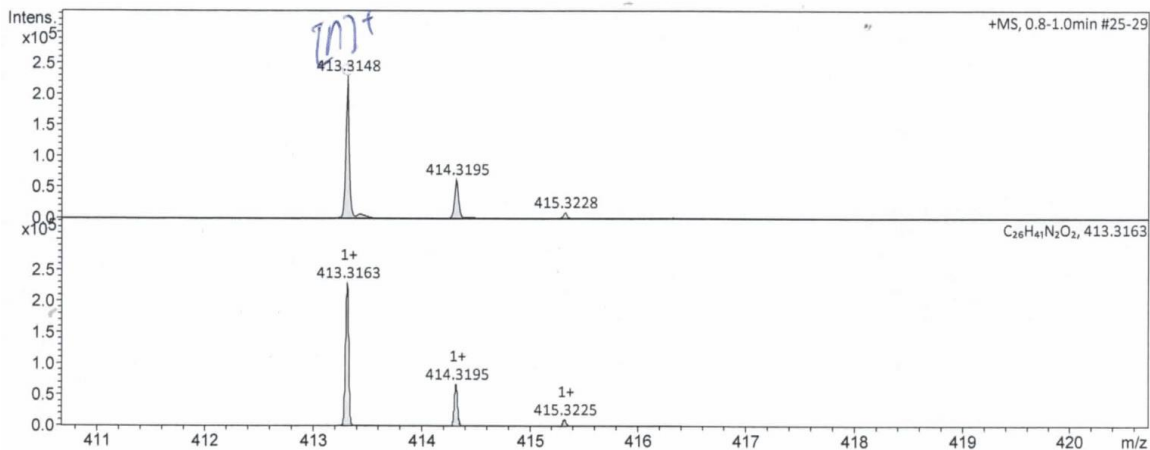
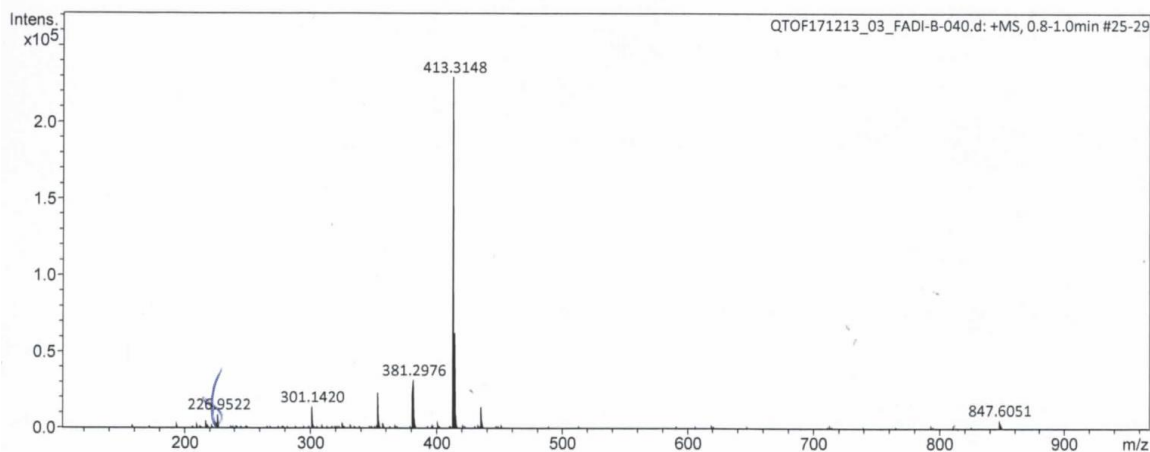
CENTRE COMMUN DE SPECTROMETRIE DE MASSE

**Analysis Info**

Analysis Name QTOF171213\_03\_FADI-B-040.d  
 Method 2016\_03\_17\_Infusion\_50-1000\_pos.m  
 Comment  
 Acquisition Date 12/13/2017 10:59:22 AM  
 Instrument / Ser# micrOTOF-Q 228888.10  
 231

**Acquisition Parameter**

Source Type	ESI	Ion Polarity	Positive	Set Nebulizer	0.4 Bar
Focus	Active	Set Capillary	1000 V	Set Dry Heater	200 °C
Scan Begin	50 m/z	Set End Plate Offset	-500 V	Set Dry Gas	4.0 l/min
Scan End	1000 m/z	Set Collision Cell RF	400.0 Vpp	Set Divert Valve	Waste



Meas. m/z	Ion Formula	Sum Formula	m/z	err [ppm]	mSigma	z	Adduct
413.3148	C26H41N2O2	C26H41N2O2	413.3163	3.5	12.8	1+	M

**Figure S21.** HRMS spectra of compound **12**; related to introduction part and Table 1